Journal of Hydrology 541 (2016) 1241–1257

Contents lists available at ScienceDirect

Journal of Hydrology

journal homepage: www.elsevier.com/locate/jhydrol

Research papers

Reduced-complexity probabilistic reconstruction of alluvial aquifer stratigraphy, and application to sedimentary fans in northwestern India

Wout M. van Dijk [a,b,*], Alexander L. Densmore [a], Rajiv Sinha [c], Ajit Singh [d], Vaughan R. Voller [e]

[a] Department of Geography, Durham University, Durham, UK
[b] Faculty of Geosciences, Universiteit Utrecht, Utrecht, The Netherlands
[c] Department of Earth Sciences, Indian Institute of Technology Kanpur, Kanpur, India
[d] Faculty of Engineering, Department of Earth Science & Engineering, Imperial College, London, UK
[e] Department of Civil, Environmental, and Geo-Engineering, National Center for Earth Surface Dynamics, Saint Anthony Falls Laboratory, University of Minnesota, Twin Cities, Minneapolis, MN, USA

ARTICLE INFO

Article history:
Received 1 March 2016
Received in revised form 8 August 2016
Accepted 15 August 2016
Available online 20 August 2016
This manuscript was handled by P. Kitanidis, Editor-in-Chief, with the assistance of Niklas Linde, Associate Editor

Keywords:
Numerical model
Alluvial aquifers
Aquifer-body connectivity
Fan system

ABSTRACT

Generating a realistic model of subsurface stratigraphy that fits data from multiple well locations is a well-established problem in the field of aquifer characterisation. This is particularly critical for the alluvial fan-hosted aquifers in northwestern India, as they have some of the highest rates of groundwater extraction in the world and spatially limited subsurface observations. The objective of this study is to develop a reduced-complexity model that generates probabilistic estimates of aquifer body occurrence within a sedimentary fan, based loosely on the northwestern Indian aquifer system. We propose a parsimonious, inverse-weighted random walk model that reconstructs potential channel belt pathways within a discrete depth range or slice by (i) connecting known aquifer locations with the fan apex, (ii) filling adjacent cells with non-aquifer material based on estimated channel-body dimensions, and (iii) random filling of the remaining cells until the model fraction of aquifer material is comparable to the bulk aquifer fraction observed from well data. Once filled, individual depth slices can be stacked to produce a three-dimensional representation of aquifer-body geometry, allowing informed inference and testable predictions about the configuration of aquifer units in the subsurface. A receiver operating characteristic (ROC) curve shows that the model performs better than fully random filling, both in matching the locations of aquifer material in the subsurface and in reconstructing the geometry of relict channel bodies preserved on the fan surface. The model differs from purely statistical-empirical approaches by incorporating some geomorphic knowledge of fluvial channel belt geometry within the fan system. In contrast to a fully process-based approach, the model is computationally fast and is easily refined as new subsurface data become available.

1. Introduction

Reconstruction of subsurface stratigraphy based on spatially-limited borehole data is a well-established problem in the field of aquifer characterisation. This reconstruction is particularly challenging for alluvial aquifer systems that consist of fluvial channel deposits, in which the major aquifer units comprise stacked sand-rich channel belts associated with alluvial fans or meandering river channels. Such settings are marked by high subsurface heterogeneity in aquifer-body characteristics and distribution due to frequent avulsion and migration of the active channel during deposition. Information derived from geophysical profiles, cores, well logs and well-test data is rarely sufficient (due to limited spatial coverage) to determine the three-dimensional geometry, size, and connectivity of aquifer bodies within these settings. These aspects of the system are critical, however, because they control aquifer volume, potential yield, and flow rates, and thus both aquifer performance and sustainability (Larue and Hovadik, 2006; Renard and Allard, 2013). Connectivity in particular is related to the existence of pathways between aquifer bodies that enable fast flow and transport from one location to another (Renard and Allard, 2013). There is a pressing need for simple, flexible, and predictable models that can simulate or anticipate these pathways. The paucity of subsurface data in many alluvial aquifer systems, and the predominance of elongate channel-body aquifers, preclude simple lateral correlation between aquifer bodies

* Corresponding author at: Faculty of Geosciences, Universiteit Utrecht, PO Box 80115, 3508 TC Utrecht, The Netherlands.
E-mail address: woutvandijk@gmail.com (W.M. van Dijk).

http://dx.doi.org/10.1016/j.jhydrol.2016.08.028
0022-1694/

recorded in different wells, whilst the lack of detailed lithological data, including age constraints, may preclude the use of more sophisticated forward models that could simulate aquifer-system deposition and development.

Previous approaches to this problem can be divided into structure-imitating, process-imitating, and descriptive methods (Koltermann and Gorelick, 1996; de Marsily et al., 2005). Structure-imitating methods, including spatial statistical and object-based methods, rely on spatial patterns in sediments and hydraulic properties, probabilistic rules, and deterministic constraints based on geometric relations within aquifers (Koltermann and Gorelick, 1996). Statistical structure-imitating methods include traditional two-point kriging or conditional methods (e.g., Isaak and Srivastava, 1990; Journel, 1988) and modern multi-point statistical (MPS) methods (e.g., Guardiano and Srivastava, 1993; Caers, 2001; Strebelle, 2002; Wu et al., 2008; Comunian et al., 2012; Rezaee et al., 2013; Mariethoz and Lefebvre, 2014). MPS methods offer a way to model complex and heterogeneous geological environments through the use of training images, which represent conceptual statistical models of the geology that has to be simulated. Whilst MPS methods are able to describe richer and arguably more realistic models than two-point methods, they have several shortcomings (Wingate et al., 2015): MPS is a purely statistical approach and requires suitable training images, which may provide model outcomes that are statistically plausible but physically unrealistic. In contrast, object-based methods use geometric or probabilistic rules, such as random walk approaches (Price, 1974) or random avulsions (Jerolmack and Paola, 2007), to mimic depositional facies seen in nature (Koltermann and Gorelick, 1996). A geological record is simulated either through rules based on conceptual depositional models and geologic principles, or through initial conditions, boundary conditions, and inputs such as sea level curves, subsidence histories, and sediment supplies (see review in Koltermann and Gorelick, 1996).

Process-imitating methods (e.g., Karssenberg et al., 2001; Pyrcz et al., 2005; Sylvester et al., 2011; Nicholas et al., 2016; Van de Lageweg et al., 2016a) are algorithms that solve a set of governing equations that mimic the processes of sediment transport and deposition in sedimentary basins and build stratigraphy (Koltermann and Gorelick, 1996). In contrast to structure-imitating methods, process-imitating methods simulate physical processes and therefore have the potential to predict realistic subsurface geometries and distributions of channel-belt sand bodies (Mackey and Bridge, 1995). In process-based models, the depositional surface is updated at each time step under the influence of both depositional and erosional processes. This makes it difficult to condition the outcome with observed data (Karssenberg et al., 2001; Wingate et al., 2015), because initial deposits may fit the data but are later erased. In addition, full fluid-dynamical simulations are too slow for simulating long-term basin development, as they use too much computational power to iteratively fit observed data. An important drawback of even simplified process-imitating models is that they still need several parameters, which may or may not be either physically-based or independently known. Also, process-based models ideally require quantitative stratigraphic information, including depositional ages and subsidence rates, in order to make systematic comparisons between model outputs and real systems.

Descriptive methods produce images of subsurface stratigraphy by combining site-specific and regional data with conceptual models (e.g., Allen, 1978; Galloway, 1981; Miall, 1985; Nemec and Steel, 1988) and insights (Koltermann and Gorelick, 1996; Van de Lageweg et al., 2016b). Descriptive methods split the aquifer into characteristic units that are based equally on hydraulic measurements and geologic observations (Fogg, 1986; Anderson, 1989). Characteristic units for reconstructing aquifer corridors are often based on the distinction between heterogeneous fluvial deposits such as gravel or sand-rich channel deposits (assumed to be aquifer material) and silt or clay-rich floodplain deposits (assumed to be non-aquifer material) (Miall, 1988; Jordan and Pryor, 1992; Willis and Tang, 2010).

In the field of fluvial routing systems, e.g., fans and deltas, hybrid models combining elements of structure-imitating and process-imitating approaches have also been successfully applied to reconstruct depositional fan settings. For example, several studies have recognised the connection between avulsion processes in fluvial sediment routing systems and the stratigraphy of channel sand bodies in the field (e.g., Price, 1974; Leeder, 1978; Allen, 1979; Bridge and Leeder, 1979; Bridge and Mackey, 1993). Thus, avulsion processes have been included, partly as probabilistic rules, in several reduced-complexity models (e.g., Price, 1974; Mackey and Bridge, 1995; Karssenberg et al., 2001; Jerolmack and Paola, 2007; Liang et al., 2015a). Such models have been used to reconstruct channel-belt deposits from the apex of the system to downstream locations based on a random walk, the local gradient and an avulsion probability that is dependent upon sediment input and changes in base level. Even these simplistic rules can produce flow velocities and water surface slopes (Liang et al., 2015b) and subsurface stratigraphic records (Karssenberg et al., 2001; Jerolmack and Paola, 2007; Liang et al., 2015b) that are comparable to the outputs of more sophisticated process-based models of fluvial routing systems. These fan models are, however, rarely used to reconstruct fan deposits from actual well log information.

Robust reconstruction of subsurface stratigraphy has major implications for our understanding of the aquifer system in northwestern India, which suffers from some of the highest rates of groundwater over-exploitation and water-level decline in the world (Rodell et al., 2009; Chen et al., 2014, 2016). Accurate geological characterisation of the aquifer system has been hampered by a lack of subsurface data; even basic first-order knowledge of aquifer-body dimensions and subsurface distribution is lacking at a regional scale. Van Dijk et al. (2016) identified two major fan systems in the region, and provided a descriptive conceptual model for the aquifer bodies that inferred the likely aquifer distribution based on some well log information and our understanding of fan systems. This conceptual model is insufficiently detailed, however, to populate local or regional hydrogeological models, and provides only statistical descriptions of the full three-dimensional stratigraphy. Because of the size of the region (44,000 km^2) and the spatial variation in aquifer body fraction (Van Dijk et al., 2016) there is no suitable geological model or three-dimensional training image that could inform a pure statistical structure-imitating approach. The study area is also so large that conditioning of the data is difficult and time-consuming, and the lack of suitable constraints on stratigraphic geometry and age control make it difficult to apply process-imitating models.

Here we propose a physically-based heuristic model that predicts the potential aquifer body distribution through incorporating our best process understanding of how the aquifer system forms into a reduced-complexity model. Our approach occupies the 'middle ground' identified by Liang et al. (2015b) between detailed and physically-explicit simulation on the one hand and abstract simplification on the other. The model is based on the deposition of continuous sandy channel material within the sediment fans that comprise the major aquifer systems in northwestern India, but we do not explicitly simulate channel transport and depositional processes. Instead, we use geological and geomorphological information on the downstream continuity and lateral discontinuity of the channel bodies, combined with a random-walk approach, to reconstruct the most likely aquifer locations in a given depth slice. We then show how two-dimensional sediment routing assumptions in a given

depth slice can be used to build a three-dimensional picture of the subsurface stratigraphy. We compare model predictions of aquifer-body positions and connectivity to the null case of random filling of the basin, and consider the implications of the model for groundwater exploration and management.

2. Study area

The study area comprises the sediment fans deposited by the Sutlej and Yamuna Rivers within the Himalayan foreland basin. The area is bounded by the Himalaya to the north, the Thar Desert to the south, and the incised valleys of the Sutlej and Yamuna to the west and east, respectively (Fig. 1). At present, sediment flux into the foreland is dominated by the Sutlej and Yamuna Rivers, as well as by smaller, foothills-fed and plains-fed river systems such as the Ghaggar River (Van Dijk et al., 2016).

Available data on aquifer-body thickness and location consist of 243 aquifer-thickness logs from the Central Groundwater Board (CGWB). These logs make a binary division of the subsurface into aquifer and non-aquifer units, and provide the depth and thickness of each layer as estimated from electrical logs by the CGWB. The logs have a median spacing of 7 km (Van Dijk et al., 2016). All of the logs extend to at least 200 m below ground level, and we therefore restrict our analysis to the top 200 m of the subsurface, noting that there is no evidence that aquifers deeper than 200 m have yet been tapped in this region.

Van Dijk et al. (2016) mapped different geomorphic units and showed a direct correlation between these units and the bulk characteristics of the underlying aquifer bodies (Fig. 1). Van Dijk et al. (2016) showed that, across the Sutlej and Yamuna sedimentary fan systems, individual aquifer bodies have a median thickness of 6–7 m and a mean thickness of 9 m. The aquifer-body thickness distributions are heavy-tailed (Van Dijk et al., 2016), indicating that there is some persistence in aquifer location. Over larger stratigraphic intervals of more than 4–8 times the median thickness, the aquifer thickness logs show evidence of impersistence, perhaps related to avulsion and compensational filling. Van Dijk et al. (2016) inferred that the thicker aquifer deposits are formed by stacked, multi-story sand bodies, perhaps originating in part as incised-valley fills, that occupied distinct corridors originating at the fan apices. Van Dijk et al. (2016) were unable to directly observe the widths of these corridors, but inferred a maximum width of 5–10 km by analogy with surface channel-belt widths (Van Dijk et al., 2016) and thickness-width relations of Gibling (2006). The bulk aquifer fraction (f_{obs}), or ratio between aquifer and non-aquifer material, is about 0.4 for both fan systems. A major exception to this occurs in the area between the Sutlej and Yamuna fans and adjacent to the Himalayan mountain front; there, aquifer bodies are both thinner and less abundant, and the bulk aquifer fraction (f_{obs}) is about 0.3. Van Dijk et al. (2016) also showed that the aquifer-body thickness distribution does not change significantly with depth, which suggests that the morphodynamics and depositional conditions of the Sutlej and Yamuna sediment routing systems have remained consistent over the time required to deposit at least the upper 200 m of the subsurface stratigraphy. The bulk aquifer fraction decreases away from the

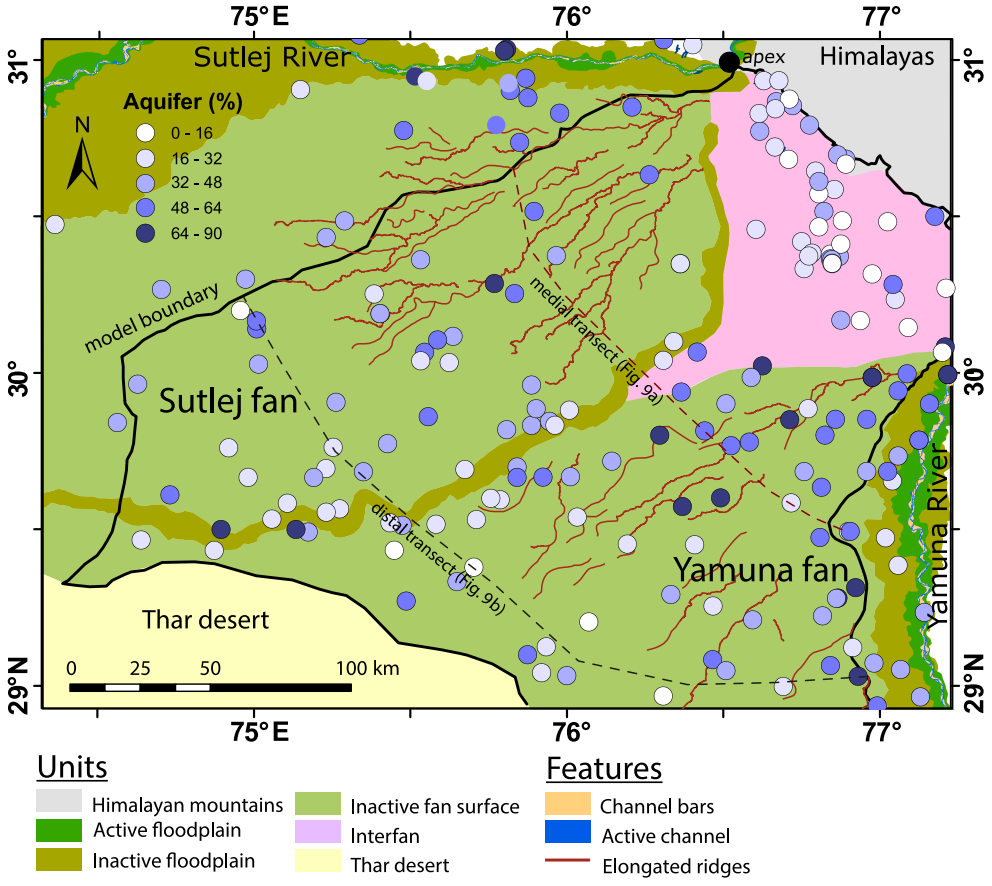

Fig. 1. Geomorphological map of the study area (modified after Van Dijk et al., 2016), covering the Sutlej and Yamuna fans and the interfan area between them (pink). Dots show locations of CGWB aquifer-thickness logs (Van Dijk et al., 2016), and colours show bulk percentage of aquifer material in the upper 200 m. The heavy black line indicates the extent of the model space, chosen to include parts of both fans. Dashed lines show the locations of medial (Fig. 9a) and distal (Fig. 9b) transects. (For interpretation of the references to colour in this figure legend, the reader is referred to the web version of this article.)

Himalayan mountain front in both the Sutlej and Yamuna fan systems, although the thickness distribution remains approximately similar, indicating that aquifer bodies make up a smaller fraction of the basin fill in the distal parts of the system but do not thin appreciably.

3. Model approach

Our modelling approach builds on the aquifer-thickness logs from the CGWB, which provide information on the presence or absence of aquifer material in the upper 200 m at 243 points across the basin. We assume that the aquifer bodies in the fan system were mainly deposited by major river channels that avulsed repeatedly across the fan surface during deposition. The likely maximum lateral dimensions of the aquifer bodies (less than 5–10 km, Table 1) are comparable to or smaller than the median spacing between adjacent logs (7 km), and Van Dijk et al. (2016) showed the difficulty of correlating between even closely-spaced boreholes, meaning that simple lateral (across-fan) extrapolation would be unwise. Similarly, whilst the river channels are continuous down-fan, channel-belt sinuosity precludes simple longitudinal correlation or extrapolation as well. For simplicity, we do not simulate the formation and filling of incised valleys in our model; whilst this is a plausible mechanism for the creation of stacked aquifer bodies like those observed in the study area, we have no data on its relative importance, and we note that its inclusion would require more complex process-based approach.

To estimate the likelihood of finding aquifer material within a given depth range between our borehole locations, we define a model space and apply a set of simple rules derived from our geomorphic understanding of fan depositional systems, including aspects such as avulsion sequence (Allen, 1978; Jerolmack and Paola, 2007), compensational filling (Sheets et al., 2002; Straub et al., 2009), and reoccupation (Stouthamer, 2005). We start by dividing the study area into a regular, square grid, with a cell size that is chosen to reflect the typical lateral dimensions of the aquifer bodies. This choice introduces an inherent length scale into the model, but is made explicitly for two reasons. First, the large median spacing between the aquifer-thickness logs means that there is no justification for a fine model grid size, as there are no data against which to validate it. Second, a relatively coarse grid obviates the need to model progressive deposition and construction of sand bodies, as would be required by a process-imitating approach. We then divide the upper 200 m of stratigraphy into regular depth slices and operate on each slice in turn. The thickness of the depth slice is chosen to be of the same order as both the median aquifer-body thickness of 6–7 m (Table 2) and the median non-aquifer unit thickness of 7.5 m. Each slice is parallel to the present topography, meaning that we assume that the modern basin surface slope is the same as the slope throughout deposition. We neglect the local surface relief, as this is typically less than 5 m, and assume that deposits at a given depth are approximately coeval. We explore the sensitivity of the model results to changes in both grid size and depth slice thickness.

The model carries out five basic operations on each depth slice: (i) identifying grid cells that contain dominantly aquifer or non-aquifer material, and filling them appropriately; (ii) establishing upstream weighted random walks between aquifer cells and the fan apex, and filling cells along those routes with aquifer material; (iii) establishing downstream weighted random walks to define aquifer corridors in both directions; (iv) filling cells adjacent to the aquifer corridors with non-aquifer material; and (v) filling the remaining empty cells randomly up to the correct bulk aquifer fraction (Fig. 2b and c). These steps are then independently repeated for successive depth slices. We then run multiple realisations of the model, and average the values in each cell to obtain probabilities of finding aquifer bodies in the subsurface.

Table 1
Observed width dimensions from the present surface (Van Dijk et al., 2016).

Basin	Feature	Width (m)
Sutlej river	Channel belt	1600–5000
Yamuna river	Channel belt	4000–10,000
Ghaggar	Paleochannel	5000–8000
Sutlej fan	Ridges	650–2300
Yamuna fan	Ridges	740–1790

3.1. Model setup

The first underpinning assumption within the model is that thick channel sands within a fan must have been deposited by a major river that entered the foreland at the fan apex, rather than by smaller foothills-fed and plains-fed river systems or reworking of fan material. This assumption is supported by the stacked, multi-story character of the aquifer bodies and by their thickness (median 6–7 m), which is much greater than the channel dimensions of smaller foothills-fed rivers like the Ghaggar River (Sinha et al., 2013; Van Dijk et al., 2016), and by provenance data that show that major channel sediments originate from the Himalayan hinterland (Singh et al., 2016). The fan apices in our study area mark the points where the Sutlej and Yamuna Rivers cross the Himalayan Frontal Thrust and enter the foreland. Whilst these points may shift over Myr time scales (e.g., Gupta, 1997; Malik and Mohanty, 2007), we assume that they have remained fixed in space over the time needed to deposit the upper 200 m of sediment in the foreland basin.

Because of the fixed position of the rivers entering the basin and the relatively thick sand bodies associated with these large river systems, we also assume that aquifer material is continuous within each depth slice between its occurrence at a point on the fan (as indicated by its appearance in the aquifer-thickness logs) and the fan apex, although not necessarily in a straight line. We then use a random walk approach to construct probable aquifer corridors in the upstream and downstream directions from those wells that contain aquifer material in that depth slice. The random walk is applied on a 2D plane, and represents the distribution of aquifer bodies within that depth slice. For simplicity, we assume that aquifer material, once deposited, is not scoured and replaced by non-aquifer deposits; we justify this by noting the evidence for stacking and persistence in channel positions over stratigraphic intervals of 4–8 times the median aquifer-body thickness (Van Dijk et al., 2016). The modelled aquifer body is, therefore, a continuous channel deposit that is connected in both the upstream and downstream directions.

To avoid unreasonably straight channels, we set weights in the upstream random walk, toward the fan apex. We apply unequal weights justified by the observed sinuosity of the modern Sutlej and Yamuna Rivers channel belts and of elongate, sand-rich ridges on the fan surfaces, interpreted as abandoned river palaeochannels by Van Dijk et al. (2016) (Fig. 2a). This analysis illustrates that, from any given cell on a river or ridge, the highest probabilities of finding an adjacent upstream river or ridge cell occur in the three cells oriented toward the fan apex (Fig. 2a).

The weighting factor for the upstream random walk is calculated by the cosine of the angle between the azimuth to each neighbouring cell and the fan apex (Fig. 2c). Thus, the weighted probability P to connect a target aquifer cell with its neighbours is defined as:

$$P = A + B\cos(C\alpha) \quad (1)$$

Table 2
Observed aquifer body thickness distribution statistics from Van Dijk et al. (2016).

Basin	Thickness percentile (m)			Total fraction	
	25th	50th	75th	Aquifer	Non-aquifer
Sutlej	4.5	7	11	0.37	0.63
Yamuna	4	6	10	0.37	0.63

where α is the angle between a straight line towards the apex and the azimuth to the neighbouring cell. The constant A is set to 0.05, representing the minimum probability observed from the elongated ridges (0.04 in Fig. 2a). The constant B is 0.35 so the maximum probability is 0.4 ($A + B$), which is based on the highest probabilities observed from the adjacent cells of the Sutlej and Yamuna river

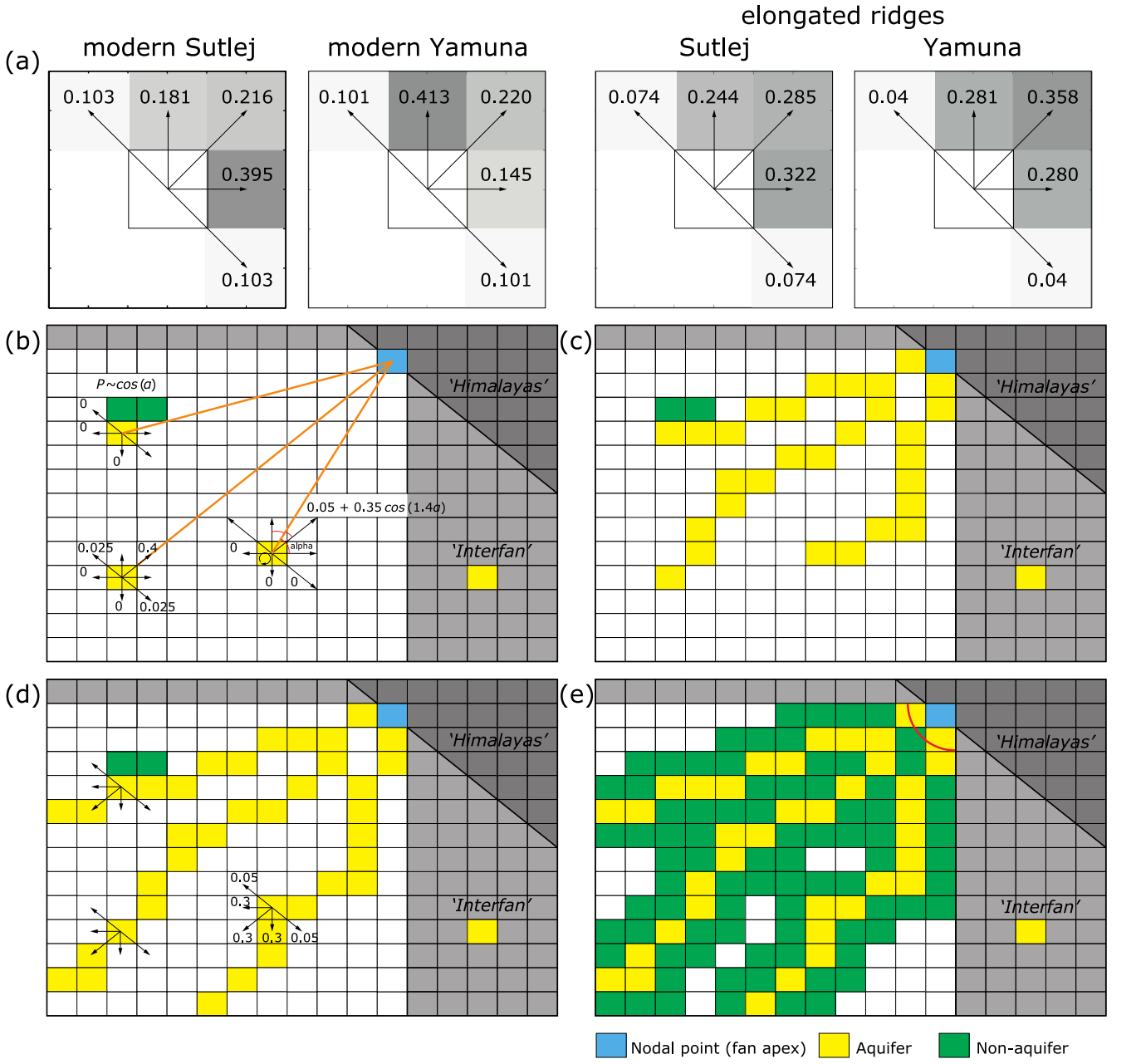

Fig. 2. Details of model algorithm and weighted random walk approach as applied in this study. (a) Directional probabilities derived from the courses of the modern Sutlej and Yamuna channel belts as well as elongate palaeochannel ridges on the Sutlej and Yamuna fans. Numbers and shading show the probabilities that the next upstream channel or ridge cell, toward the fan apex, will occur in one of the eight cardinal directions shown. Probabilities are calculated by the summation of all identified channel or ridge of the adjacent cells for all individual channel or ridge cell, where the probabilities of the cells mirrored to the three cells towards the fan apex are set to zero and probabilities of cells in the NW and SE directions are divided by two. These probabilities are converted to weights in the random walk used to populate the model with aquifer material. (b) Schematic showing how the probabilities in (a) are weighted by the angle to the fan apex, and how potential aquifer bodies are routed through the cells around known non-aquifer locations. The probability is modified by a cos(α) term, in which α is zero towards the fan apex. (c) Routing of aquifer material upstream toward the fan apex using the weighted probability. (d) Routing of aquifer material downstream with equal probabilities in the three down-fan directions. (e) Filling of non-aquifer material in the cells that are laterally adjacent to each aquifer corridor.

(0.413 in Fig. 2a). The constant C is set to 1.4 to limit the span of the random walk to 130° as observed on both the Sutlej and Yamuna fans. The weighted probability is calculated for all 8 neighbouring cells. Negative values are set to zero, and the probabilities for all directions that fall between alpha values of −90° and 90° are set to a small but arbitrary value of at least 0.025, so that the random walk has at least four upstream cells to choose. The four directions are needed as in some cases the three direct upstream grid cells for coarser grids are identified as non-aquifer from the observational data, leaving no alternative pathway toward the apex. Because P depends on α and thus on location, we rescale the values so that they sum to 1 for each set of neighbours. Also, to force connectivity between aquifer-body positions on the fan and the fan apex, the weighted random walk uses progressively higher probability values towards the apex and P is recalculated after each step. The random walk towards the apex is first calculated from well locations that are closest to the apex, and then for those that are progressively further away. We terminate each random walk when it reaches the apex or when it encounters another previously-identified aquifer cell. In the downstream direction, we apply a simplified weighting factor with equal probabilities of 0.3 to the three neighbouring cells away from the fan apex, and a small probability of 0.05 for the cells parallel to the mountain front (Fig. 2d). This simplified scheme is used because there is not a fixed location (like the fan apex) where the random walk must end. The downstream random walk is applied in reverse order, so that well locations furthest away from the fan apex are analysed first. Each walk terminates when it encounters another previously-identified aquifer cell or when it reaches the model boundary (see boundary in Fig. 1). Because the order of the random walk may affect the resultant probabilities, we also test a model in which the order was reversed, as well as a model that operates on well locations in a random sequence.

Our second assumption is that aquifer bodies, whilst continuous in the down-fan direction between the fan apex and points on the fan, are highly discontinuous in the across-fan direction. Thus, assuming that our model grid cells are sized appropriately, the presence of aquifer material in one cell should mean that there is non-aquifer material in adjacent cross-fan cells (i.e., those with alpha values of c. ±90°). This assumption is likely to be true if shifts in the active channel system across the fan occur by avulsion near the fan apex. If, instead, the channel migrates laterally during fan deposition, then aquifer material would be expected in adjacent cells with little vertical separation. The lack of clear correlations between aquifer material in adjacent boreholes in our study area, as documented by Van Dijk et al. (2016), appears to argue for a dominance of avulsion over lateral migration in this system. Thus, after connecting all aquifer cells to an upstream aquifer cell and eventually to the fan apex, all cells adjacent to those continuous aquifer corridors are filled with non-aquifer material (Fig. 2e).

After these steps, there remain some unfilled cells within the model grid – that is, cells for which we have neither direct observation nor geomorphic rules to determine whether they should contain aquifer or non-aquifer material. Our final constraint is that the bulk model aquifer fraction must match that of the actual fan system, as estimated from the aquifer-thickness logs. Thus, on the fans we fill the remaining cells with aquifer material at random until the bulk aquifer fraction matches the observed value of 0.4. Randomly-filled cells will not necessarily be adjacent or connect to the main channel corridors. Cells in the interfan area, which is not supplied by either the Sutlej or Yamuna rivers, are also filled randomly to match the observed bulk aquifer fraction of 0.3. Once the observed aquifer fraction value of 0.4 has been reached, any final remaining cells that have not been identified as aquifer cells are filled with non-aquifer material to complete the depth slice.

3.2. Model parameters and sensitivity

The model is governed by several parameters: the number of realisations, the grid cell size, the slice thickness, and the minimum aquifer thickness. Each model realisation produces a single solution of the distribution of aquifers in each depth slice, which can be thought of as a map of aquifer locations that contains only zeros (non-aquifer) and ones (aquifer). We perform Monte Carlo-type iterations to produce probabilities in the range [0,1], defined for each cell as the fraction of realisations that give rise to aquifer material in that cell. We vary the number of realisations between 1 and 250 to test how that affects the cumulative probability distribution.

Given our assumptions, the grid cell size should be limited to the typical lateral dimensions of the potential aquifer bodies. Van Dijk et al. (2016) showed that both the elongate palaeochannel ridges and the modern channel belts on the fan surfaces vary between 2 and 10 km wide, whereas channel-body thickness-width scaling relations are likely to be ~1:1000, suggesting a maximum width of about 6 km for a median aquifer-body thickness of 6 m (Gibling, 2006). We perform simulations with variable grid resolutions from 2 km to 8 km, related to the various channel width interpretations, to understand the resulting differences and uncertainties in aquifer distribution. Most of the results shown here are based on a cell size of 6 km, which relates to the median aquifer body thickness. Whilst it would certainly be possible to allow channel-belt widths to vary in space (e.g., Rongier et al., 2014), we make the simplifying assumption that they are fixed and uniform. This is justified for two reasons: we lack any data on channel-width variations in space within the subsurface of these fans, making any spatial variations arbitrary; and we do not know, a priori, whether the CGWB aquifer-thickness logs have penetrated the aquifer bodies near their centres or near their margins, so that definition of a true width in space would be very uncertain. An additional reason for using a low-resolution grid is that much of the CGWB data on aquifer performance (including estimated abstraction rate, potential evapotranspiration, and recharge) are available on, at most, a block level. The mean block area in Punjab and Haryana states is about 360 km^2 (10 model grid cells at a 6 km spacing), so there is little rationale for a substantially higher model resolution. Conversely, model outcomes and predictions can be fairly easily adapted to the block scale if required.

Likewise, the slice thickness is chosen to scale with the median (or mean) aquifer-body thicknesses observed in the Sutlej and Yamuna fan systems, which are 6–7 m and 9 m across the study area, respectively (Van Dijk et al., 2016). Slice thicknesses of 5 and 10 m give quantitatively similar simulation results for the two-dimensional aquifer network, and so for simplicity we use 10 m depth slices for most tests of model sensitivity and cross-validation. For analysis of the three-dimensional representation of subsurface aquifers, in contrast, we use 5 m depth slices as this will give a more accurate connectivity measure in the vertical direction.

The accuracy of the model is determined by the number and distribution of observations that are used to populate the known aquifer and non-aquifer grid cells in the first model step. Because aquifer-thickness logs are not evenly distributed and the distance is sometimes smaller than the grid size, multiple logs may occur in a single grid cell. For example, for a 6 km grid spacing, several log locations fall within the same cell, so that, whilst there are 208 logs on the fan surfaces, only 59 cells of the 884 cells of the Sutlej fan and 90 cells of the 695 cells in the Yamuna fan are known from the observational data. Thus, we assign each cell value based on the predominance of either aquifer or non-aquifer material in that cell and depth slice. In most cases, we assign the cell as aquifer

when at least one of the logs is composed predominantly of aquifer material within that depth slice. This approach is justified by the limited lateral extent of the aquifer bodies; logs near the centre of a body would record its full thickness, but logs near its margins would record only a portion of its total thickness and might be dominated by non-aquifer material, even in the same cell and depth slice. To test the sensitivity of our results to this approach, we also run an alternative algorithm that classifies a cell as non-aquifer if at least one of the logs is composed predominantly of non-aquifer material. We also test the extent to which the model results are influenced by thin aquifer bodies – that is, units that may reflect terminal (crevasse) splays or small plains-fed channels draining the fan surfaces rather than deposits of the major rivers, and for which our model assumptions may therefore not be valid. To do this, we run alternative model scenarios where we ignore aquifer bodies in the input logs that are thinner than the median thickness of 6–7 m when populating the model space.

3.3. Model analysis

3.3.1. Cross-validation

True validation of the model is impossible because the actual aquifer locations are unknown. Therefore, we first assess the performance of the model by applying it to a test case of a two-dimensional image of a channel network. As the test case image, we use the network of ridges on the surface of the Sutlej fan (Fig. 1), inferred by Van Dijk et al. (2016) to represent a set of abandoned sand-rich palaeochannels that radiate from the Sutlej fan apex. We interpolate these ridges onto a grid with a spacing of 2 km (similar to the maximum observed 2.3 km width of the ridges; Van Dijk et al., (2016) and classify ridge locations as aquifer material, which fills about 25% of the grid. The remainder of the grid is classified as non-aquifer material, completing the test case (Fig. 3a). We then remove a subset (80–95%) of the image at random, and use the remaining 5–20% as the starting point for our model (Fig. 3b). We compare the model results (Fig. 3c) to both the test case (Fig. 3a) and to a null model (Fig. 3d), created by simple random filling of the grid with aquifer material with the same bulk aquifer fraction; both our model and the random filling model are run 100 times. This gives a probability map for both our model (Fig. 3e) and random filling (Fig. 3f). Subsequently, the probability maps can be converted back to an aquifer location map by applying a probability threshold μ, such that probabilities above the threshold are classed as aquifer material and those below as non-aquifer. The threshold is inversely proportional to the model-predicted bulk aquifer fraction (f_μ); high thresholds will yield low aquifer fractions, and vice versa.

To quantitatively compare these probability maps, with values in the range of [0,1], we calculate receiver operating characteristic (ROC) curves to assess the model fit to the reserved subset of palaeochannel positions. The ROC curve is a graphical plot that illustrates the performance of a binary classifier system (in this case, aquifer and non-aquifer) as the probability threshold μ is varied. The curve is created by plotting the true positive rate (TPR), defined as the number of cells that are aquifer in both the predictive model and the data divided by the number of actual aquifer cells, against the false positive rate (FPR), defined as the number of cells that are aquifer in the predictive model but non-aquifer in the data divided by the number of non-aquifer cells. The TPR and FPR are calculated for various values of μ. Increasing μ leads to fewer cells being classified as model aquifers, and should lead to a decrease in both TPR and FPR. ROC curves are constructed for both the model outputs and random filling of the grid. An effective model should show a higher TPR at a given FPR than random filling, and the TPR should also improve as a larger fraction of the available data is used to generate the model.

Comparison of the model results with the test case tests the ability of the model to produce aquifer corridors comparable to the elongated ridges in terms of their spatial distribution. Testing the ability of the model to generate a realistic distribution of potential aquifer bodies in the subsurface is more complicated, as we lack full three-dimensional information on aquifer bodies across the study area. We therefore assess the model performance by removing a random subset (10–50%) of the CGWB aquifer-thickness logs to use as a test data set before running the model. We then compare the model predictions at the test log positions against the actual observations. To avoid any potential bias introduced by our choice of test logs, we run 50 simulations with different subsets of test logs. The outcomes are then compared to a random filling approach using the ROC curves. Furthermore, we also construct separate ROC curves for the proximal (<100 km from the fan apex) and distal (>100 km from the fan apex) parts of the fans, to investigate whether the model performance is position-dependent.

3.3.2. Subsurface stratigraphy and connectivity

To compare the model outcomes for multiple realisations with the statistical analysis of aquifer thickness data of Van Dijk et al. (2016), we need to create a three-dimensional representation of the subsurface stratigraphy. Therefore, we stack the individual depth slices and apply the probability threshold μ to convert aquifer probability to the presence or absence of aquifer material. The value of μ is chosen so that the model-predicted bulk aquifer fraction (f_μ) of the multiple realisations is the same as the bulk aquifer fraction (f_{obs}) of the CGWB aquifer-thickness data. Aquifer-body thicknesses are then calculated for all grid cell locations from the stacked depth slices and compared to the aquifer-body thicknesses from the original logs. To examine the spatial distribution of potential aquifer bodies, we also extract medial and distal cross sections oriented parallel to the Himalayan mountain front (see Fig. 1 for locations). The medial transect includes logs that are located 50–110 km from the mountain front, whilst the distal transect includes logs that are 160–250 km from the mountain front.

The three-dimensional stack from the multiple realisations also contains information about the connectivity of the potential aquifer bodies within the subsurface. Aquifer-body connectivity directly affects pumping or recovery, especially in regions with an intermediate proportion of aquifer bodies (Allen, 1978; Renard and Allard, 2013) such as our study region. Because the model builds potential aquifer bodies that are continuous down-fan and are surrounded by non-aquifer material, horizontal connectivity is to an extent hard-wired into the model outputs. The vertical connectivity is not pre-determined, however, nor is the connectivity between adjacent aquifer corridors. Here, we test model (multiple realisations) connectivity for various values of μ, compared to the results of random filling. We characterise these by the model-predicted bulk aquifer fraction (f_μ), which is inversely proportional to μ, as this makes it possible to directly compare the outcomes from our model with random filling. The range in μ for random filling is smaller and is generally lower compared to our model. We characterise connectivity by applying a commonly-used scalar index Γ that defines the probability of connection between two potential aquifer body cells (Larue and Hovadik, 2006; Hovadik and Larue, 2007), and is calculated as:

$$\Gamma = \frac{\sum_{i=0}^{n}(V_i^2)}{\left(\sum_{i=0}^{n} V_i\right)^2} \quad (2)$$

where V_i is the volume of an individual body and n is the total number of potential aquifer bodies. In the case of a single aquifer body,

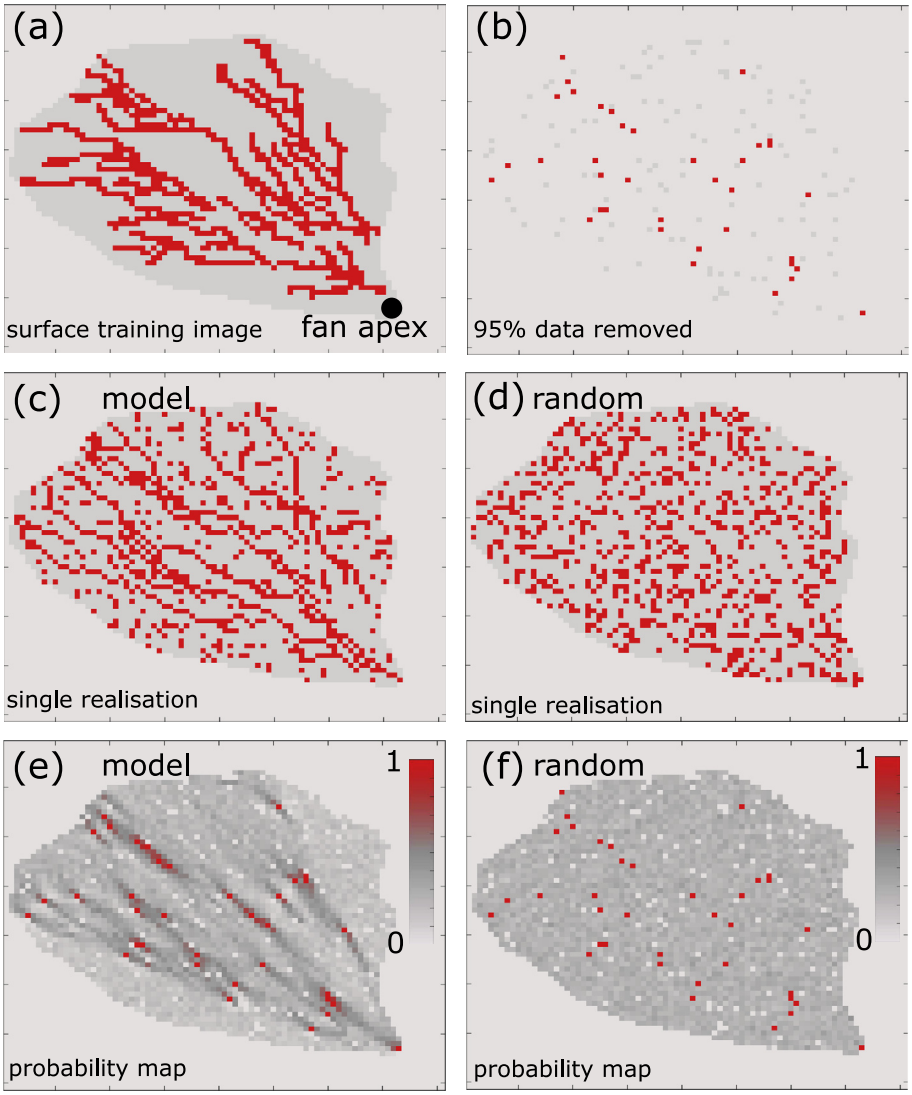

Fig. 3. (a) Test case of the elongated ridges, used to assemble a quantitative measure of the precision of the model in reconstructing the aquifer pathways. Red cells show ridge locations. (b) In the next step, 95% of the image is removed, leaving 5% of the cells filled with aquifer or non-aquifer material. (c) Example of a single realisation with our model. Red cells show cells filled with aquifer material. (d) Example of a single realisation of random filling of the cells up to 25% with aquifer material. (e) Probability map based on 100 realisations from our model. (f) Probability map based on 100 realisations from random filling. (For interpretation of the references to colour in this figure legend, the reader is referred to the web version of this article.)

this probability is 1, as the volume of the single aquifer is equal to the total aquifer-body volume. As the number of aquifers increases, or equivalently as the bulk aquifer fraction increases, the connectivity index is initially low but then increases as clusters of connected aquifer bodies are formed (Stauffer and Aharony, 1992; Christensen and Moloney, 2005; Hovadik and Larue, 2007). High connectivity implies fewer but larger clusters, with a high probability that any two cells are connected within a cluster (Hovadik and Larue, 2007). For example, Γ for a system of 10 individual aquifer bodies with a volume of 1 cell each will be 0.1, whereas a system with the same aquifer fraction but comprising 1 body with a volume of 10 cells will give a Γ of 1.

We allow connectivity between adjacent cells along faces, edges, and vertices (26 possibilities), although other rules give qualitatively similar results. We calculate the connectivity index for various values of μ (or equivalently for different f_μ), for both the model output and the case of random filling. We plot potential aquifer body connectivity within the subsurface stratigraphy for two down-fan sections, normal to the mountain front, and three across-fan sections parallel to the mountain front, in order to compare the two models.

4. Results

4.1. Model output

A single realisation of the model produces a map that contains only zeros and ones – that is, aquifer and non-aquifer material (Fig. 4a). Running multiple realisations yields a probability of finding aquifer material (with values in the range [0,1]) at every location within the region of interest (Fig. 4b). Increasing the number of realisations leads to a smoother cumulative probability distribution (Fig. 4c). There is little difference, however, between the cumulative probability distributions for 100 and 250 realisations (Fig. 4d). The model algorithm is coded in MATLAB, and a typical 100-realisation run for a 6×6 km grid on a standard desktop computer takes on the order of 10 s per depth slice. The aquifer probability values are affected by the processing order of the random walk. In the cases of a reversed processing order (i.e., starting with aquifer cells farthest from the apex) or a randomly-chosen sequence, aquifer pathways are more likely to be parallel toward the fan apex rather than intersecting, because the space near the apex is not filled as quickly, so that aquifer probability values are generally slightly higher.

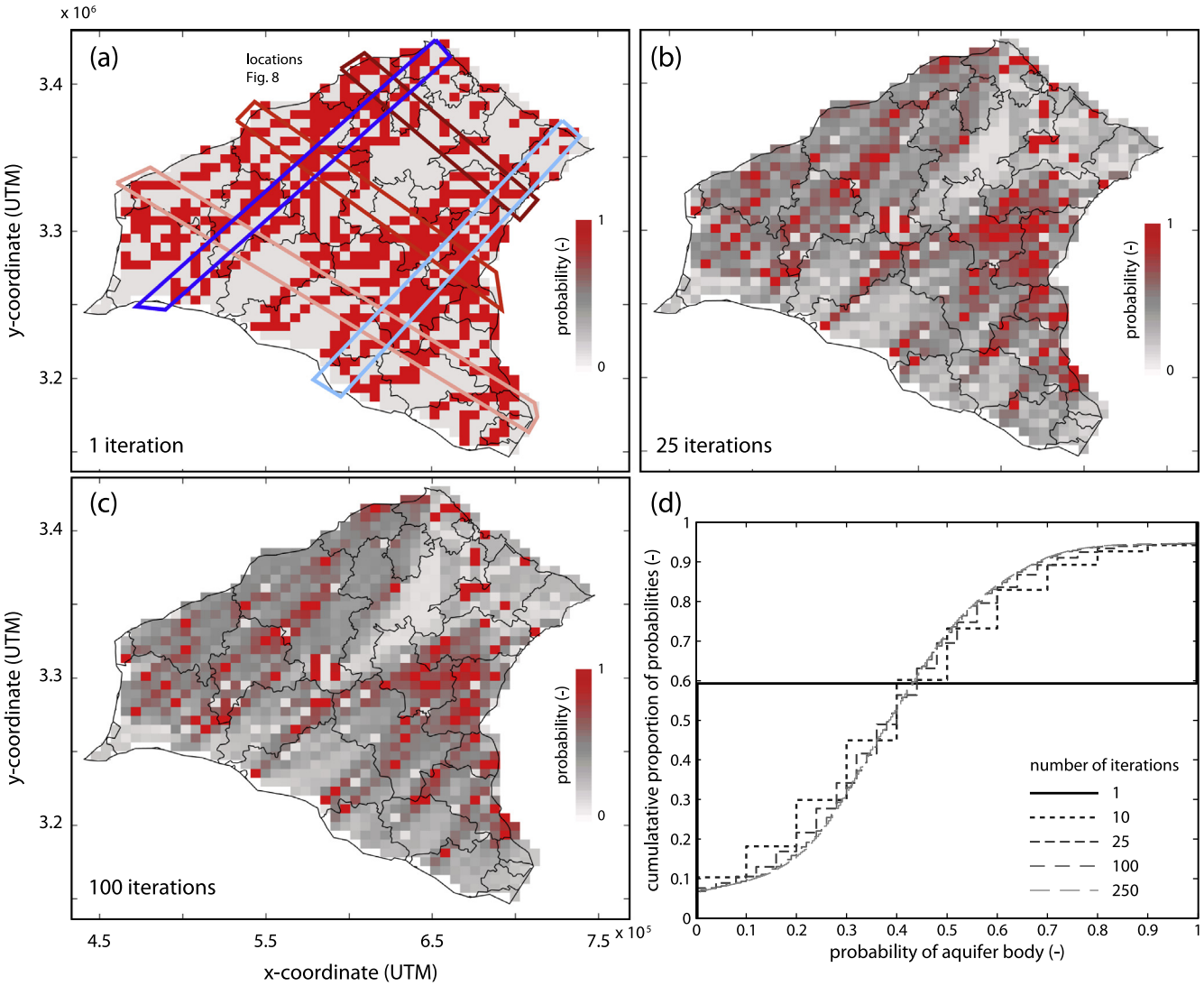

Fig. 4. (a) Results from a single model run for a single depth slice (in this case, 80–90 m below ground level) and a 6 × 6 km grid. In this and subsequent panels, the colour bar shows the probability of finding aquifer material in each cell, and the black polygons indicate district borders for reference. After a single run, the probability is either 1 (aquifer) or 0 (non-aquifer). The coloured boxes indicate the locations for the connectivity analysis shown in Fig. 8. (b) Model results after 25 iterations. 'Known' cells containing aquifer-thickness logs retain 1 or 0 values, but all other cells contain probabilities in the range [0,1]. (c) Model results after 100 iterations, showing a somewhat different pattern of probabilities. (d) The cumulative distribution of probabilities for all depth slices after different numbers of iterations. Results with 100 and 250 iterations are indistinguishable. Note that the curve does not tend to 0 or 1 because of the presence of known cells with fixed probability values. (For interpretation of the references to colour in this figure legend, the reader is referred to the web version of this article.)

4.2. Sensitivity to channel width

Most of the model runs are carried for a channel width interpretation of 6 km represented by 6 × 6 km grid cells. A decrease in the channel width, i.e., the grid size, to 2 × 2 km, equivalent to the maximum width of the elongated fan surface ridges (Table 1), shows that the probability of finding aquifer material at any given cell generally decreases (Fig. 5a), and provides some additional information on the likelihood of finding potential aquifer bodies within the large-scale corridors identified on the lower-resolution grid (Fig. 4c). Runs for smaller channel widths, i.e., higher grid resolutions, also yield larger uncertainties for points that are well away from the known log locations. Reducing the channel width and increasing the number of grid cells also means that a larger area must be randomly filled to obtain a bulk aquifer fraction of 0.4 on the fans (Fig. 5b). This effect is not straightforward, though, because of the geometry of the potential aquifer bodies in the model. Although the number of cells is increased by a factor of 9 for a 2 × 2 km grid compared to the base configuration, the fraction of empty cells is only increased by 4.5 times (Fig. 5b). This is because, with a coarser grid, the spacing between two adjacent aquifer corridors may be less than 2 grid cells, so that fewer adjacent cells are filled with non-aquifer material compared to the finer grid.

4.3. Sensitivity to the input data

Reconstruction of aquifer corridors depends on the precedence given to the input data. When a cell is classified as aquifer material, then a corridor is created and propagated upstream and downstream, but when a cell is classified as dominantly non-aquifer material, then there are no rules that are used to set the surrounding cells. This affects the number of empty cells after applying our model rules and eventually the number of cells that

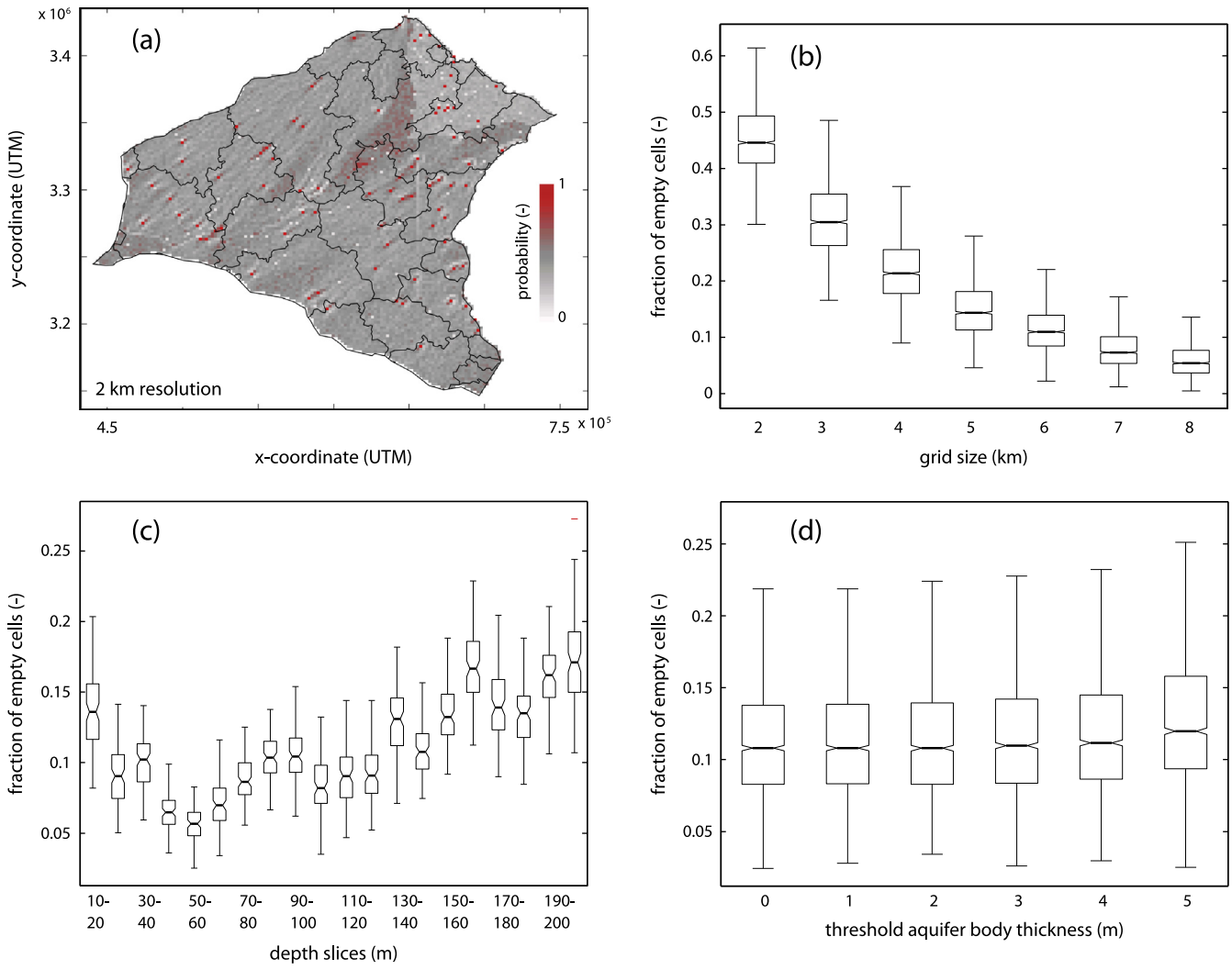

Fig. 5. Controls on the fraction of empty cells that must be filled by the model. (a) Model results using a 2 × 2 km grid and 100 iterations. Compared with Fig. 4, probabilities are more distributed, with fewer dominant corridors of high aquifer probability. (b) Decline in the number of empty cells that must be filled by the model with increasing grid cell size. Boxes show median, 25th and 75th percentiles, and error bars show ±1 standard deviation for 100 iterations at each cell size. (c) Variability in the number of empty cells in each 10 m depth slice for 100 iterations. The number of empty cells depends on the aquifer percentage in the input data for each depth slice. (d) The fraction of empty cells for runs that ignore aquifer bodies that are less than a given threshold in thickness. This change has no significant effect on the fraction of empty cells.

are randomly filled. Thus, the number of empty cells varies with depth slices, showing fewer empty cells for the top 100 m (Fig. 5c). Further, there are more empty cells (that must then be randomly filled) when non-aquifer material is given precedence for cells with multiple logs (Fig. 6a). This change causes a decline in the high aquifer probabilities associated with connected aquifer corridors on both fans (see the blue colours in Fig. 6b).

Assignment of a cell as aquifer or non-aquifer material is based on aquifer bodies that vary in thickness from 1 m up to 80 m. Whilst it is unlikely that the thinnest aquifer bodies were deposited by major river systems that were connected with the fan apex (as required by our model assumptions), simulations that ignore aquifer bodies of less than 6 m thickness show no significant changes in the number of empty cells left in the model or in the overall pattern of aquifer probabilities (Fig. 5d). This means that the same area is filled by our algorithm, i.e., the model outcome is not greatly affected by the thinnest aquifer bodies, probably because they make up a small fraction of each 10 m depth slice.

4.4. Model performance cross-validation

The ROC curves allow us to examine three separate aspects of the model: the effect of the threshold μ used to convert aquifer probability into aquifer presence or absence, the effect of the removal of an increasing proportion of the input logs to validate the model results, and the differences in performance between the model and random filling. In the case of random filling, increasing the threshold (that is, increasing the probability value needed to assign aquifer material to a cell in the final map) causes a proportionate decrease in both TPR and FPR, so that the ROC curve is approximately a straight line (Fig. 7a). The model, however, performs better for increasing threshold values, as shown by the increasing ratio of TPR to FPR (Fig. 7a–d). Removal of an increasing fraction of the input data has little effect on the ROC curves in the case of random filling, as it causes little relative change in the number of cells that are randomly filled (Fig. 7a–c). For the model, however, removal of an increasing fraction of input data causes the ROC curves to shift noticeably towards the random filling curves, because a greater number of cells must be filled randomly.

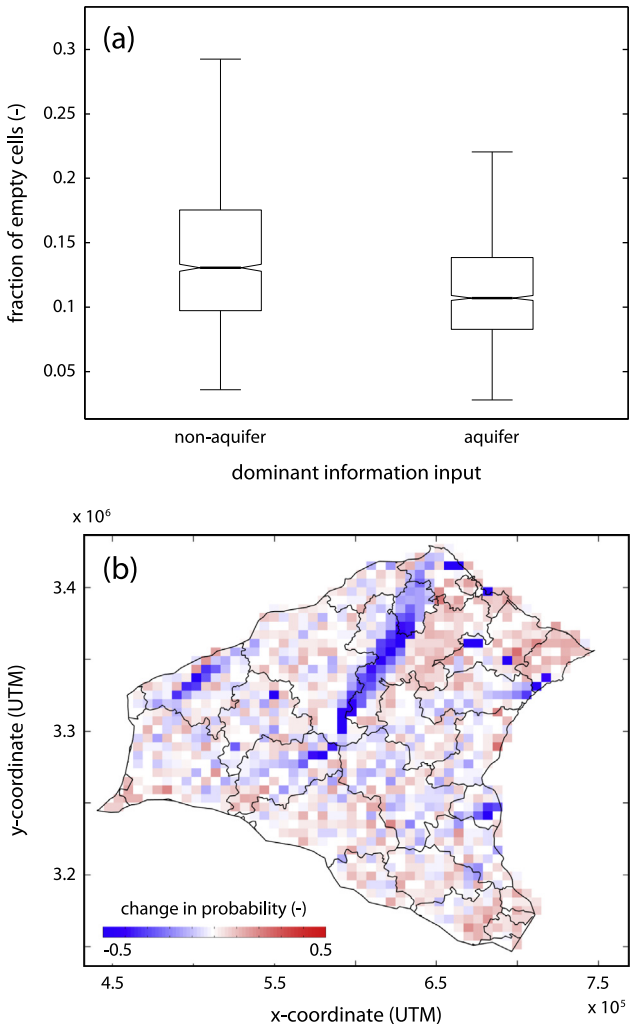

Fig. 6. (a) The effect of dominance in the input data when multiple well logs occur within a single grid. For runs marked 'aquifer', a cell is classified as aquifer if the majority of at least one input log consists of aquifer material within that depth slice. For runs marked 'non-aquifer', a cell is classified as non-aquifer if the majority of at least one input log consists of non-aquifer material. The cell size is 6×6 km, and the model was run for 100 iterations. Note that non-aquifer precedence results in the assignment of a smaller number of aquifer cells, and thus a larger number of empty cells that must be filled randomly. (b) Spatial pattern of changes in aquifer probability when using aquifer material, rather than non-aquifer material, as the dominant input. The blue colour illustrates the reduction in aquifer probability when the non-aquifer information is dominant. Note that the blue colour follows one of the major aquifer pathways in Fig. 4c. (For interpretation of the references to colour in this figure legend, the reader is referred to the web version of this article.)

Overall, the model shows a higher TPR-FPR ratio than the case of random filling for high probability thresholds, particularly when used to reproduce the elongate palaeochannel ridges on the Sutlej fan (Fig. 7a). Random filling yields a higher TPR than the model, however, for low threshold values, especially for the CGWB input logs (Fig. 7b and c). A total of 50 simulations including different randomly-chosen subsets of the data shows that the model generally performs very well compared to random filling, with a TPR of 0.5 over a FPR of 0.2. However, selecting a different subset of the data could lead to a poor solution as well (Fig. 7c), but overall the model performs better than random filling. Comparison of the ROC curves from different parts of the fan shows that the TPR-FPR ratio is higher, especially for conservative threshold values, i.e., when FPR is low, for the proximal part of the fan (Fig. 7d). This means that model performance, relative to the case of random filling, is somewhat reduced for distal locations.

4.5. Sand-body connectivity

A single realisation of the model forms elongate 'ribbons' that are, by design, well-connected in the down-fan direction, but less so in the across-fan direction. Unfortunately, we cannot compare the connectivity of our model after multiple realisations results with independent connectivity estimates. Instead, we examine the sensitivity of the connectivity index to the threshold μ (or f_μ), and determine the μ value at which the model output behaves as an isotropic aquifer. We compare the model results (Fig. 8) to results from the case of random filling along several different cross sections.

The potential aquifer bodies created by the model are generally more connected than those generated by random filling, except at low values of μ, equivalent to high f_μ (Fig. 8a). In both cases, the index increases rapidly for moderate f_μ, as isolated potential aquifer bodies become clustered. This transition occurs at f_μ of 0.1–0.3 for the model as well as for random filling (Fig. 8a). This analysis shows that for both approaches, potential aquifer bodies are highly isotropically connected for f_μ of 0.4 or greater.

The model predicts that aquifer body connectivity in the down-fan direction should be similar to or greater than connectivity in the across-fan direction, as we would expect to see in a fan system, especially for f_μ values of 0.4 or greater (Fig. 8b). At lower f_μ, the model predicts greater across-fan connectivity, especially in proximal and medial sections compared in distal sections (Fig. 8b). Thus, we should expect a greater degree of across-fan connectivity near the fan apices, because potential aquifer bodies are constrained to converge at the apex and combine to a big aquifer with high connectivity. The proximal section, however, is less connected as expected because of low values in the interfan area between both fan systems. In contrast, random filling of aquifer material gives rise, unsurprisingly, to connectivity that is essentially isotropic in both the down-fan and across-fan directions (Fig. 8c), and is unable to reproduce the connectivity patterns that we might expect in fan settings.

5. Discussion

The model simulations yield probability maps of finding aquifer locations within a series of depth slices. Stacking the depth slices together gives information on the likely spatial distribution of high aquifer probabilities in the subsurface. We first relate the modelled distribution to our expectation of fan stratigraphy in general, and our understanding of the Sutlej-Yamuna fan system (Van Dijk et al., 2016) in particular. We also consider the possible uses and limitations of the model, and some ideas for how it could be improved.

5.1. Relation between model results and subsurface stratigraphy of the Sutlej-Yamuna fans

Recall that the model contains no specific rules about sediment transport, depositional processes, or fan construction; instead, it uses some knowledge of the lateral and vertical dimensions of individual aquifer bodies along with their spatial disposition. Because the model rules are focused on individual aquifer units, it is not necessarily clear that the model-derived stratigraphy – which consists of a stack of individual aquifer units – will provide a physically-reasonable representation of regional stratigraphy. Thus, it is instructive to compare the model stratigraphy with both a theoretical expectation of fan stratigraphy and our observations of subsurface aquifer-body distributions in the study area (Van Dijk et al., 2016). To do this, the model outputs for each 5 m depth slice are stacked to represent the probabilistic aquifer-body

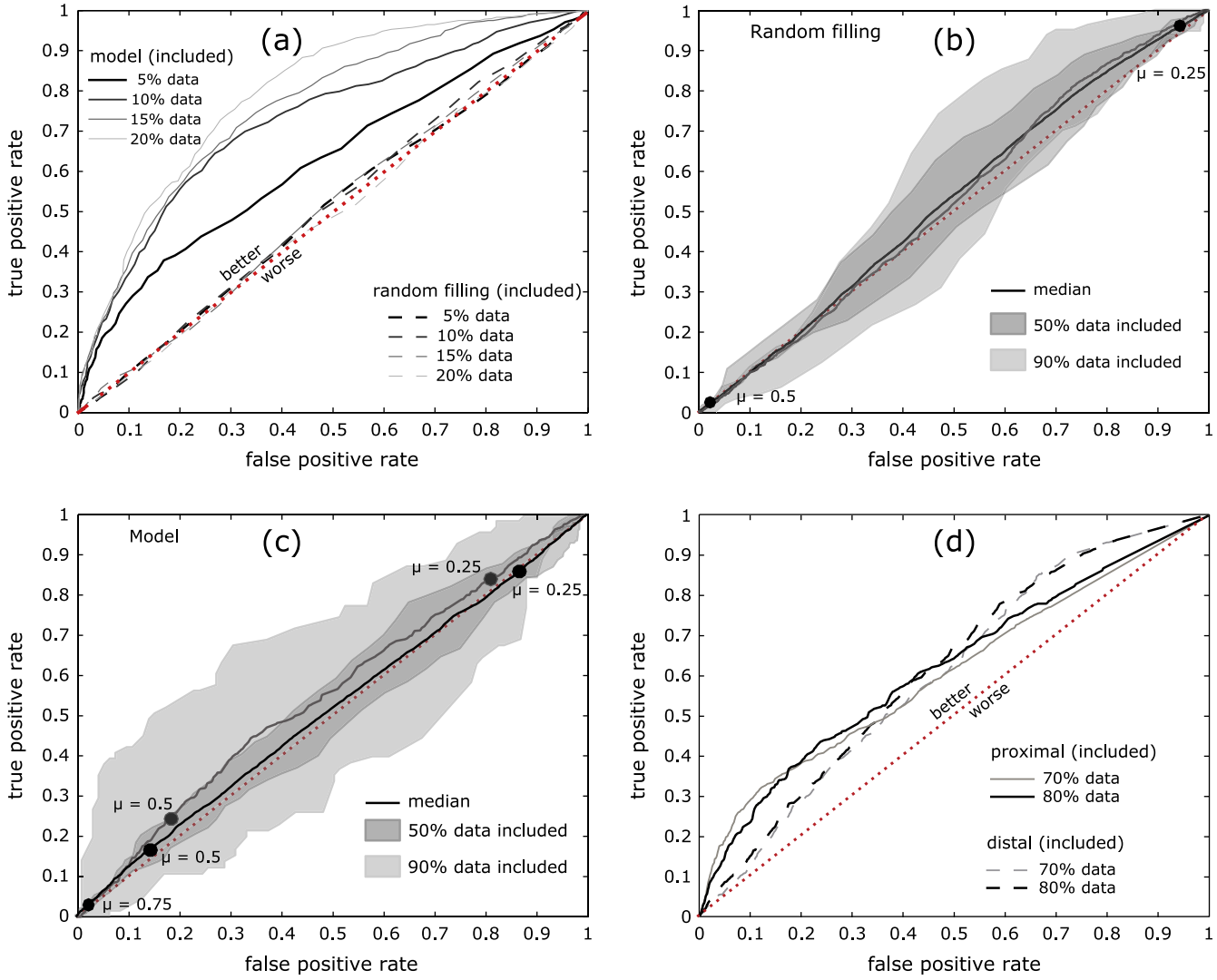

Fig. 7. Quantitative characterisation of the performance of the model compared to the case of simple random filling. (a) ROC curves showing the ability of both model (solid lines) and random filling (dashed lines) to reproduce the positions of elongated ridges on the Sutlej fan surface (the test case). The true positive rate (TPR) shows the proportion of cells that are aquifer material in both the simulated output and the test case, whilst the false positive rate (FPR) shows the proportion of cells that are aquifer material in the simulation but non-aquifer in the test case. A perfect model would plot in the upper left-hand corner (TPR = 1, FPR = 0). The curves are derived by increasing the probability threshold value from 0 (upper right-hand corner, all aquifer material) to 1 (lower left-hand corner, no aquifers). Different lines show simulations with varying proportions of the input data included, to compare with the model results. The model consistently has a higher TPR-FPR ratio than random filling for all threshold values. (b) ROC curves showing the ability of random filling to reproduce a reserved set of input CGWB aquifer-thickness logs. The solid line shows the median output for 50 simulations and the shaded area shows the range between the best and worst simulations. Selected probability thresholds are shown on each curve for reference. c, ROC curves showing the ability of the model to reproduce a reserved set of input logs. Symbols as in panel (b). Note that the region of low FPR, i.e., corresponding to moderate to high values of the probability threshold, would be appropriate for a conservative assessment of the model. In this region, the model has generally a higher TPR-FPR ratio than random filling, especially when more data are included. d, ROC curves showing the ability of the model to reproduce the reserved set of input CGWB logs for both proximal locations (solid lines, within 100 km of the fan apex) and distal locations (dashed lines, more than 100 km from the apex). The TPR-FPR ratio is higher for the proximal part of the fan systems for the region of low FPR and moderate to high values of the probability threshold.

distribution for the top 200 m of the subsurface. We then apply a threshold μ to transform the probability values to modelled potential aquifer bodies in a three-dimensional volume. The size and spatial pattern of those bodies is dependent on the applied μ, such that potential aquifer bodies are both thicker and more numerous for a lower μ (Table 3). For a μ of 0.45, meaning that a modelled aquifer cell is simulated as aquifer material in at least 45% of the iterations, the quantiles of the aquifer thickness distribution (25th, 50th and 75th percentiles) as well as the f_μ are closest to their observed values based on the aquifer-thickness logs (Table 2, Van Dijk et al., 2016). Interestingly, this μ also corresponds to the highest ratio of TPR to FPR within the ROC curve (Fig. 7b). We therefore apply this μ in our further analysis of the modelled potential aquifer bodies below.

Conceptual fan models often indicate a general decrease in the lateral dimensions of the sand bodies in downstream direction (e.g., Friend, 1978; Nichols and Fisher, 2007; Cain and Mountney, 2009; Weissmann et al., 2013; Owen et al., 2015). Near the fan apex, we would expect little preservation of associated fine-grained overbank deposits, and channel deposits are likely to be stacked or amalgamated (Friend, 1983). Away from the apex, conceptual models predict that the proportion of overbank deposits should increase and the dimensions of channel deposits should decrease. In agreement with this expectation, the interpolated aquifer probabilities are generally higher along the medial transect (Fig. 9a) compared to the distal transect (Fig. 9b). Both transects, but especially the medial one, contain high probabilities of aquifer material along corridors that are collectively more than 6 km wide,

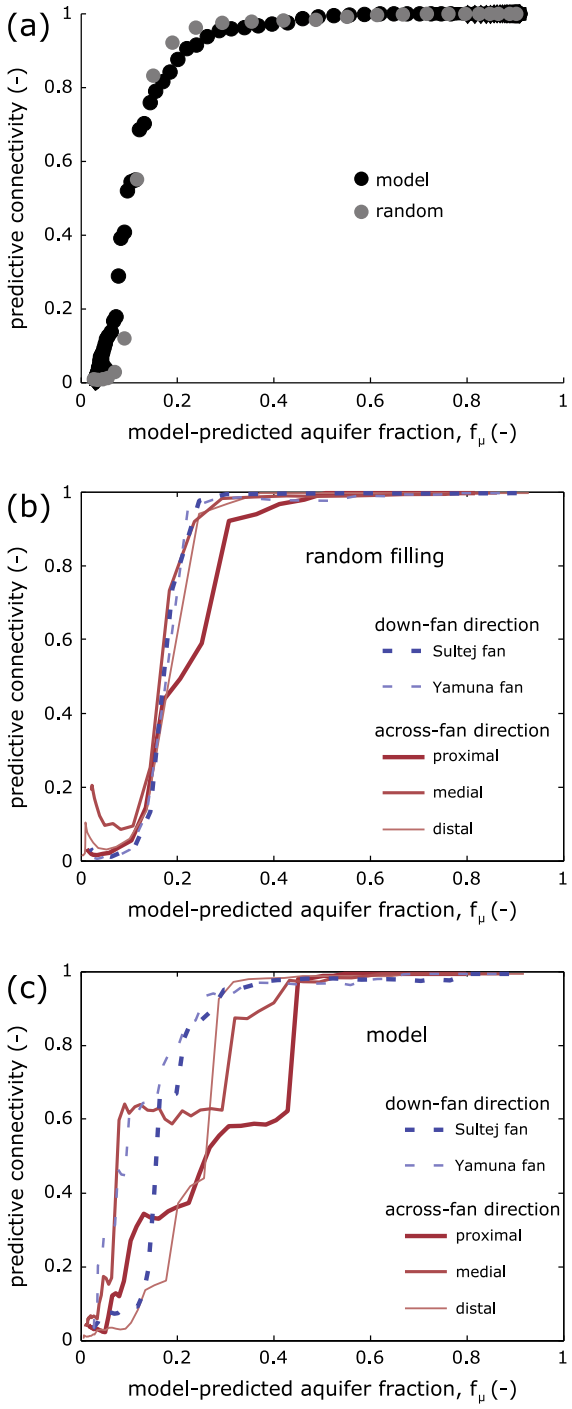

Fig. 8. (a) Smoothed isosurfaces of model potential aquifer bodies for a probability threshold value of 0.45. The aquifer material forms a set of 'ribbon'-shaped bodies that are elongate down-fan, away from the Sutlej and Yamuna fan apices. Note that the smoothed isosurfaces are created for visualisation purposes by interpolation of aquifer cells, and are therefore somewhat thicker and wider than the actual data that are used for the analysis. Coloured boxes indicate areas used to evaluate connectivity both parallel to transport (down-fan direction, blue) and normal to transport (across-fan direction, red). (b) Variation in the connectivity index with increasing f_μ, equivalent to an increasing probability threshold value. Symbols show connectivity along faces, edges, and vertices (26 possibilities). Model connectivity (black symbols) is higher than that for random filling (grey symbols) at low f_μ, typical of the study area. (c) Variations in the connectivity index along faces, edges and vertices for the model as a function of f_μ, taken along the transects shown in panel (a). Connectivity in the down-fan direction is generally equal to, or greater than, that in the across-fan direction, and connectivity in proximal parts of the system is greater than that in distal areas. At high f_μ, however, connectivity is high and essentially isotropic. (d) As panel (c), but for the case of random filling. Connectivity is essentially isotropic at all f_μ. (For interpretation of the references to colour in this figure legend, the reader is referred to the web version of this article.)

i.e., more than the grid resolution associated with 6 km wide channel belts. These corridors could be due to (i) amalgamation of multiple individual potential aquifer bodies, (ii) interpolation onto the transect, oblique to the grid direction, or (iii) interpolation of multiple realisations creating high probabilities around known well locations. An alternative approach that would reduce interpolation effects would be to use an object-based model, combining the random walk to define the channel pathways with an assumption about channel belt width and thickness at each point. This approach has been successfully applied to construct 3D karst conduits in the subsurface (Rongier et al., 2014).

Conceptual fan models also suggest that a downstream decrease in aquifer-body thickness should be expected because of channel termination or bifurcations (e.g., Friend, 1978; Nichols and Fisher, 2007). Owen et al. (2015) showed, however, that for Jurassic fan systems of the Morrison Formation in the western USA, the channel size did not significantly change down fan but that the percentage of fines increased. This is also observed in the Yamuna fan but less in the Sutlej fan (Van Dijk et al., 2016); the aquifer thickness distribution remains similar with distance from the fan apices, but the fraction of aquifer bodies decreases. Van Dijk et al. (2016) interpreted this pattern as a simple volumetric consequence of the conical fan shape combined with a near-uniform size of the aquifer bodies across the study area, perhaps due to stacking of channel belts or filling of incised valleys. A similar analysis of the aquifer-body thickness distribution derived from the model results shows no decrease in aquifer-body thickness down fan, similar to the observations from the Yamuna fan (Table 4). It must be remembered that our model aquifer thicknesses are multiples of 5 m, so that quantitative comparisons with real aquifer-thickness distributions must be made with caution.

Fan models also encompass the connectivity of sand bodies within the subsurface stratigraphy, which enables fast flow and transport from one location to another (Larue and Hovadik, 2006; Renard and Allard, 2013). Horizontal connectivity is partially set by the model rules, because we assume that individual bodies are continuous down-fan, are no more than one grid cell in width, and are bounded by finer-grained non-aquifer material, but in practice the horizontal connectivity depends also on the density of aquifer cells in the input data. The extent of vertical connectivity between the bodies should increase as the probability threshold μ (which controls the model-predicted bulk aquifer fraction, f_μ) is increased. Our analysis shows that sand bodies for both approaches are fairly well connected throughout the basin (Fig. 8b), but the connectivity differs in cross-fan and down-fan direction for our model compared to random filling (Fig. 8c and d). Our model has reasonably high connectivity in the cross-fan direction, despite the fact that the model is actually hard-wired against cross-fan connection. There is no difference in connectivity between our model and random filling for aquifer systems with a bulk aquifer fraction (f_{obs}) of more than ~0.5 (Fig. 8c and d). This suggests that the model has no additional skill for predicting connectivity within a highly sand-dominated system – for example, the Kosi fan in northern India, with a bulk aquifer fraction of 0.89 (Sinha et al., 2014).

5.2. Potential use and future improvements of the model

The model provides a tool to estimate the probability of finding aquifer material within a near-surface volume, based on information at known well locations and some simplified geological knowledge about the origin, depositional pattern, and likely dimensions of aquifer bodies. The model could be used in a generic sense to understand the potential variations in subsurface aquifer distribution and connectivity in cases of variable bulk aquifer

Table 3
Modelled aquifer body thickness distribution statistics for various μ values.

Basin	μ	5-m interval			f_μ	10-m interval			f_μ
		Thickness percentile (m)				Thickness percentile (m)			
		25th	50th	75th		25th	50th	75th	
Sutlej	0.3	5	15	40	0.79	10	20	70	0.77
	0.35	5	15	30	0.68	10	20	60	0.68
	0.4	5	10	25	0.51	10	20	50	0.56
	0.45	5	10	20	0.34	10	20	40	0.42
	0.5	5	10	15	0.21	10	20	40	0.28
	0.55	5	10	15	0.13	10	20	30	0.20
Yamuna	0.3	5	15	35	0.75	10	20	50	0.67
	0.35	5	15	30	0.64	10	20	40	0.57
	0.4	5	10	25	0.48	10	20	40	0.48
	0.45	5	10	20	0.34	10	20	40	0.38
	0.5	5	10	20	0.23	10	20	40	0.31
	0.55	5	10	15	0.15	10	20	40	0.24

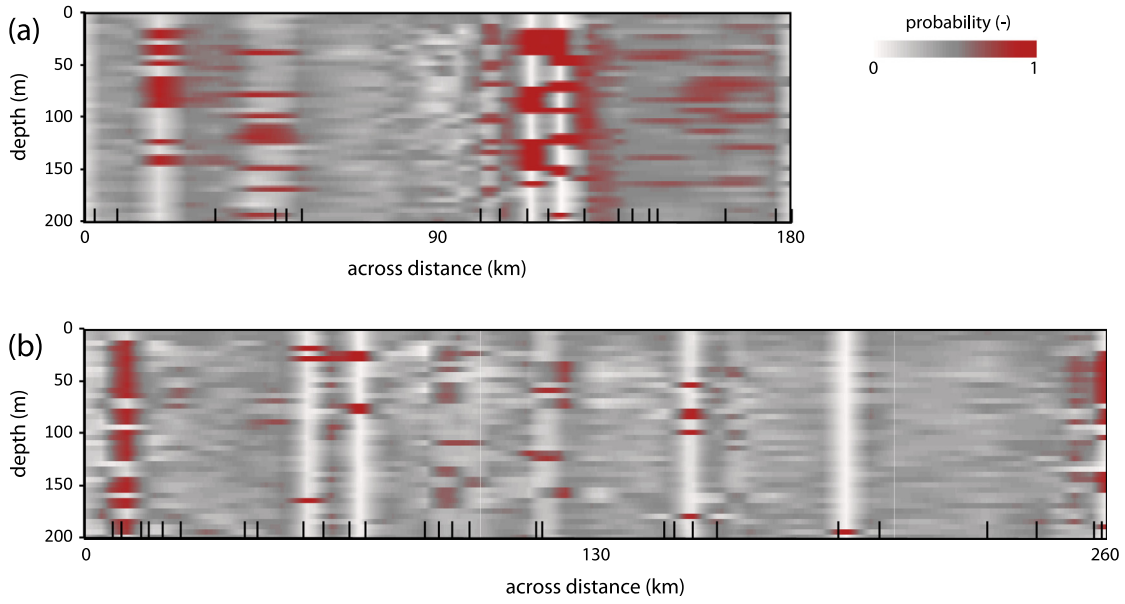

Fig. 9. Model probabilities of finding aquifer material along (a) the medial transect and (b) the distal transect, extracted from a model with a grid size of 6 × 6 km, 5 m depth slices, and 100 iterations. The model yields high probabilities at locations near aquifer-thickness logs, whereas areas without borehole information are more likely to be classified as non-aquifer material. Probabilities are overall smaller for the distal transect compared to the medial transect. See Fig. 1 for transect locations.

Table 4
f_{obs} with distance from the fan apex for the CGWB data and f_μ for the 25th, 50th, and 75th percentiles from the model results.

Basin	Distance	f_{obs}	f_μ		
		Fraction	25th	50th	75th
Sutlej	0–50	0.47	0.25	0.53	0.83
	50–100	0.45	0.23	0.35	0.53
	100–150	0.37	0.20	0.30	0.45
	150–200	0.29	0.20	0.30	0.43
	200–250	0.34	0.19	0.30	0.48
Yamuna	0–50	0.41	0.38	0.46	0.58
	50–100	0.38	0.25	0.50	0.78
	100–150	0.42	0.25	0.43	0.65
	150–200	0.29	0.15	0.28	0.43
	200–250	0.26	0.13	0.21	0.36

fractions. Because we have populated the model with actual data on aquifer-body positions taken from the CGWB aquifer-thickness logs, however, it is also useful as a predictive tool to generate probabilities of encountering aquifer bodies at any point, and at any given depth, across the study region. The model algorithm strikes a balance between purely empirical (and computationally simple) approaches on the one hand, and process-based but more computationally-intensive approaches on the other. Because of its simplicity, it can easily be updated to incorporate new subsurface information on aquifer-body positions (e.g., from new boreholes),

as that simply increases the number of 'known' cells at the start of the model run. There is no need to redefine the geometry of potential aquifer bodies or channel pathways in the subsurface, as that is done automatically, and because model run times are short the model can be quickly re-run to reflect evolving knowledge.

Encouragingly, the model performs best when compared to random filling at low false-positive rates, corresponding to a high value of the probability threshold μ that is used to convert aquifer probability into the presence or absence of model aquifers (Fig. 7b and c). A conservative strategy for identifying target areas for new wells would seek to minimise false-positives (i.e., locations where the model predicts aquifer material at a given depth, but none is found), and under those constraints the model substantially outperforms random filling. The model could thus be employed as a guide to prioritise the siting of new wells. It could be combined with, for example, magnitude-frequency analysis of aquifer-thickness data (Van Dijk et al., 2016) to also provide information on the probability of encountering an aquifer body of a given thickness at those new well locations. The more specific effects of the 3D subsurface stratigraphy generated by the model on groundwater flow and transport, and the quantitative differences between model stratigraphy and that generated by random filling, would need to be tested with regional-scale hydrogeological modelling (e.g., Ronayne and Gorelick, 2006; Burns et al., 2010). It would also be useful to perform groundwater flow and transport simulations on the various individual realisations instead of the probability maps, which could for example yield information on uncertainty in contaminant propagation prediction. This application might need refinement of the grid to avoid numerical artefacts. Refinement could be done either for individual realisations or by adapting our model algorithm. For example, we could apply the algorithm on a finer grid, then fill adjacent cells perpendicular to the random walk to obtain an aquifer width of 6 km before continuing our algorithm.

There are a number of areas of the model that could be improved or refined. The surface test case of the elongated ridges shows that there is good performance when 10% of the fan area is covered with data. However, the performance for the subsurface is less accurate. The two different data sets are recording different things; the ridges are fluvial, open fan channels, whilst the reserved logs are recording aquifer bodies. We have inferred that the surface ridges are a good analogue for subsurface channel bodies because of their scale and pattern (radiating from the fan apex). The subsurface, however, contains some incised-valley fills, which may not be represented by the surface ridges, and which may have different preservation potential in the subsurface (Weissmann et al., 1999).

Whilst the regional coverage of our aquifer-thickness data is extensive, the logs are still relatively sparse, and the model is forced to fill many gaps even on our low-resolution 6×6 km grid. This grid spacing is based on likely aquifer-body widths as inferred from surface observations in the study area (Van Dijk et al., 2016). There is substantial uncertainty on those widths, stemming from both the range of channel deposit widths visible at the surface and the viability of surface features as an appropriate analogue for subsurface aquifer bodies. For example, the elongated surface ridges that are used as an analogue for subsurface channel deposits are only 500–2500 m wide (Van Dijk et al., 2016), meaning that a 2–3 km grid might allow for more precise delineation of potential aquifer bodies. This would lead, however, to a dramatic increase in the number of empty cells that the model must fill (Fig. 5b), and clearly we lack the subsurface data to test the advantages of a more precise model result in any quantitative way. The ROC curve shows that the distal part of the fan is already less accurately predicted with the current data availability (Fig. 7d). Poor model performance could also be caused by the fact that we neglect the local surface topography and assume that the modern basin surface slope is the same as the slope throughout fan deposition. An improvement would be to obtain actual local surface topography and use a different reference elevation for connecting the various logs. Finally, we caution that the model algorithm, whilst flexible and potentially portable to other fan settings, has been designed with the Sutlej-Yamuna fan system in mind. At the very least, application to other fans would require some preliminary analysis of available aquifer-thickness data and observations of channel-belt dimensions and deposit widths, in order to set both the depth slice thickness and model grid size to appropriate values. The model sensitivity to the bulk aquifer fraction (Figs. 7 and 8) also shows that, for systems with a high aquifer fraction, the model provides little additional information or skill over simple random filling, because the likelihood of finding aquifer material is high everywhere. Thus, application to this type of fan system, such as the Kosi fan, does not appear warranted.

6. Conclusions

We have shown that the subsurface distribution of aquifer corridors across the Sutlej and Yamuna fans in northwestern India can be reconstructed by a reduced-complexity probabilistic model that incorporates some degree of geological knowledge of the depositional system. The model connects known locations of aquifer material with the fan apex by a weighted random walk, and uses the assumed lateral dimensions of the major aquifer bodies to identify likely locations of non-aquifer material to either side of the aquifer corridors. The model is sensitive to the type and distribution of input information, and the addition of new subsurface data can cause a substantial decrease in the number of empty cells that must be filled by the model. Cross-validation of the model against a subset of input CGWB aquifer-thickness logs indicates that the model provides an increase in the true-positive rate compared to simple random filling of the basin, especially for moderate to high values of the threshold used to convert aquifer probability into model aquifer position.

The model produces a simplified representation of the subsurface stratigraphy across the study area that matches key aspects of the spatial distribution of aquifer thicknesses (Van Dijk et al., 2016). The results show that aquifer-body probability is highest near the fan apices, as multiple channel systems must be routed through a relatively small area, compared with lower probabilities in distal regions. This high probability in proximal regions is also reflected in the high connectivity between potential aquifer bodies in the across-fan direction, normal to the transport direction, despite the fact that the model rules militate against lateral connectivity. In general, predicted aquifer connectivity is higher and more anisotropic for the model-derived stratigraphy than for the case of random filling, especially at low to moderate bulk aquifer fractions like those found in the study area.

The model could be used to explore variations in aquifer-body distribution at different aquifer fractions, or to predict the likelihood of finding aquifer material at a given location and depth across the study region. Importantly, model performance increases as more data are incorporated, meaning that information from new boreholes could be used to iteratively increase the model accuracy as new parts of the system are explored. The model could also be applied to other fan-hosted aquifer systems, although some caution is needed in ensuring that the geological rule set remains valid and that appropriate model dimensions are chosen.

Acknowledgements

This project is supported by the UK Natural Environment Research Council and the Indian Ministry of Earth Sciences under

the Changing Water Cycle-South Asia program (Grant NE/I022434/1). We gratefully acknowledge Sanjeev Gupta for many helpful and insightful discussions. We thank Tejdeep Singh of the Central Groundwater Board, Chandigarh, for providing the aquifer thickness data for Punjab and Haryana. Constructive and positive reviews by Meredith Reitz and two anonymous reviewers, Associate Editor Niklas Linde, and Editor Peter Kitanidis helped to clarify and strengthen the manuscript. To obtain the data and Matlab code used in this paper, please contact the authors.

References

Allen, J.R.L., 1978. Studies in fluviatile sedimentation: an exploratory quantitative model for the architecture of avulsion-controlled alluvial studies. Sed. Geol. 21, 129–147. http://dx.doi.org/10.1016/0037-0738(78)90002-7.

Allen, J.R.L., 1979. Studies in fluviatile sedimentation: an elementary gegeometric model for the connectedness of avulsion-related channel sand bodies. Sed. Geol. 24, 253–267. http://dx.doi.org/10.1016/0037-0738(79)90072-1.

Anderson, M.P., 1989. Hydrogeologic facies models to delineate large-scale spatial trends in glacial and glaciofluvial sediments. Geol. Soc. Am. Bullet. 101, 501–511.

Bridge, J.S., Leeder, M.R., 1979. A simulation model of alluvial stratigraphy. Sedimentology 26, 617–644. http://dx.doi.org/10.1111/j.1365-3091.1979.tb00935.x.

Bridge, J.S., Mackey, S.D., 1993. A revised alluvial stratigraphy model. In: Marzo, M., Puigdefabregas, C. (Eds.), Alluvial Sedimentation. International Association of Sedimentologists Special Publication, pp. 319–336.

Burns, E.R., Bentley, L.R., Hayashi, M., Grasby, S.E., Hamblin, A.P., Smith, D.G., Wozniak, P.R.J., 2010. Hydrogeological implications of paleo-fluvial architecture for the Paskapoo Formation, SW Alberta, Canada: a stochastic analysis. Hydrogeol. J. 18, 1375–1390. http://dx.doi.org/10.1007/s10040-010-0608-y.

Caers, J., 2001. Geostatistical reservoir modelling using statistical pattern recognition. J. Petrol. Sci. Eng. 29, 177–188.

Cain, S.A., Mountney, N.P., 2009. Spatial and temporal evolution of a terminal fluvial fan system: the Permian Organ Rock Formation, South-east Utah, USA. Sedimentology 56, 1774–1800. http://dx.doi.org/10.1111/j.1365-3091.2009.01057.x.

Chen, J., Famigliett, J.S., Scanlon, B.R., Rodell, M., 2016. Groundwater storage changes: present status from GRACE observations. Surv. Geophys., 1–21 http://dx.doi.org/10.1007/s10712-015-9332-4.

Chen, J., Li, J., Zhang, Z., Ni, S., 2014. Long-term groundwater variations in Northwest India from satellite gravity measurements. Global Planet. Change 116, 130–138. http://dx.doi.org/10.1016/j.gloplacha.2014.02.007.

Christensen, K., Moloney, N.R., 2005. Complex and criticality. Advanced Physics Texts, vol. 1. Imperial College Press, London, pp. 15–29.

Comunian, A., Renard, P., Straubhaar, J., 2012. 3D multiple-point statistics simulation using 2D training images. Comp. Geosci. 40, 49–65. http://dx.doi.org/10.1016/j.cageo.2011.07.009.

Fogg, G.E., 1986. Groundwater flow and sand body interconnectedness in a thick multiple-aquifer system. Water Resour. Res. 22, 679–694.

Friend, P.F., 1978. Disdistinct features of some ancient river systems. In: Miall, A.D. (Ed.), Fluvial Sedimentology, Memoirs of the Canadian Society of Petroleum Geologist, pp. 531–542.

Friend, P.F., 1983. Towards the flield classification of alluvial architecure or sequence. In: Collinson, J.D., Lewin, J. (Eds.), Modern and Ancient Fluvial Systems. IAS Special Publication, pp. 345–354. http://dx.doi.org/10.1002/9781444303773.ch28.

Galloway, W.E., 1981. Depositional Architecture of Cenozoic Gulf Coastal Plain Fluvial Systems, vol. 31. SEPM Special Publication, pp. 127–155.

Gibling, M.R., 2006. Width and thickness of fluvial channel bodies and valley fills in the geological record: a literature compilation and classification. J. Sed. Res. 76, 731–770. http://dx.doi.org/10.2110/jsr.2006.060.

Guardiano, F., Srivastava, R.M., 1993. Multivariate geostatistics: Beyond bivariate moments. In: Soares, A. (Ed.), Proceedings of the 4th Annual International Geostatistical Congres – Geostatistics Troia '92. Kluwer Academic Publishers, Norwel, Massachusetts, USA, pp. 133–144.

Gupta, S., 1997. Himalayan drainage patterns and the origin of fluvial megafans in the Ganges foreland basin. Geology 25, 11–14.

Hovadik, J.M., Larue, D.K., 2007. Static characterization of reservoirs: refining the concepts of connectivity and continuity. Petrol. Geosci. 13, 195–211.

Isaak, E.H., Srivastava, R.M., 1990. An Introduction to Applied Geostatistics. Oxford University Press, New York, USA.

Jerolmack, D.J., Paola, C., 2007. Complexity in a cellular model of river avulsion. Geomorphology 91, 259–270. http://dx.doi.org/10.1016/j.geomorph.2007.04.022.

Jordan, D.W., Pryor, W.A., 1992. Hierachical levels of heterogeneity in a Mississippi River meander belt and application to reservoir systems. AAPG Bullet. 76, 1601–1624.

Journel, A., 1988. Fundamentals of Geostatistics in Five Lessons. American Geophysical Union, Washington, DC, USA. http://dx.doi.org/10.1029/SC008.

Karssenberg, D., Törnqvist, T.E., Bridge, J.S., 2001. Conditioning a process-based of sedimentary architecture to well data. J. Sed. Res. 71, 868–879.

Koltermann, C.E., Gorelick, S.M., 1996. Heterogeneity in sedimentary deposits: a review of structure-imitating, process-imitating, and descriptive approaches. Water Resour. Res. 32, 2617–2658.

Larue, D.K., Hovadik, J., 2006. Connectivity of channelized reservoirs: a modelling approach. Petrol. Geosci. 12, 291–308. http://dx.doi.org/10.1144/1354-079306-699.

Leeder, M.R., 1978. A quantitative stratigraphic model for alluvium, with spatial reference to channel deposit density and interconnectedness. In: Miall, A.D. (Ed.), Fluvial Sedimentology. Canadian Society of Petroleum Geologists Memoir, pp. 587–596.

Liang, M., Geleynse, N., Edmonds, D.A., Passalacqua, P., 2015a. A reduced-complexity model for river delta formation – part 2: assessment of the flow routing scheme. Earth Surf. Dynam. 3, 87–104. http://dx.doi.org/10.5194/esurf-3-87-2015.

Liang, M., Voller, V.R., Paola, C., 2015b. A reduced-complexity model for river delta formation – part 1: modeling deltas with channel dynamics. Earth Surf. Dynam. 3, 67–86. http://dx.doi.org/10.5194/esurf-3-67-2015.

Mackey, S., Bridge, J., 1995. Three-dimensional model of alluvial stratigraphy: theory and application. J. Sed. Res. 65B, 7–31.

Malik, J.N., Mohanty, C., 2007. Active tectonic influence on the evolution of drainage and landscape: geomorphic signatures from frontal and hinterland areas along the Northwest Himalaya, India. J. Asian Earth Sci. 29, 604–618. http://dx.doi.org/10.1016/j.jseaes.2006.03.010.

Mariethoz, G., Lefebvre, S., 2014. Bridges between multiple-point geostatistics and texture synthesis: review and guidelines for future research. Comp. Geosci. 66, 66–80. http://dx.doi.org/10.1016/j.cageo.2014.01.001.

de Marsily, G., Delay, F., Gonçalvès, J., Renard, P., Teles, V., Violette, S., 2005. Dealing with spatial heterogeneity. Hydrogeol. J. 13, 161–183. http://dx.doi.org/10.1007/s10040-004-0432-3.

Miall, A.D., 1985. Architectural-element analysis: a new method of facies analysis applied to fluvial deposits. Earth-Sci. Rev. 22, 261–308.

Miall, A.D., 1988. Reservoir heterogeneities in fluvial sandstones: lessons from outcrop studies. AAPG Bullet. 72, 682–697.

Nemec, W., Steel, R.J., 1988. What is a fan delta and how do we recognize it? In: Nemec, W., Steel, R.J. (Eds.), Fan Deltas: Sedimentology and Tectonic Settings, pp. 3–13.

Nicholas, A.P., Sambrook Smith, G.H., Amsler, M., Ashworth, P.J., Best, J.L., Hardy, R.J., Lane, S.N., Orfeo, O., Parsons, D.R., Reesink, A.J.H., Sandbach, S.D., Simpson, C.J., Szupiany, R.N., 2016. The role of discharge variability in determining alluvial stratigraphy. Geology 44, 3–6. http://dx.doi.org/10.1130/G37215.1.

Nichols, G.J., Fisher, J.A., 2007. Processes, facies and architecture of fluvial distributary system deposits. Sed. Geol. 195, 75–90. http://dx.doi.org/10.1016/j.sedgeo.2006.07.004.

Owen, A., Nichols, G.J., Hartley, A.J., Weissmann, G.S., Scuderi, L.A., 2015. Quantification of a distributive fluvial system: the Salt Wash DFS of the Morrison Formation, SW USA. J. Sed. Res. 85, 544–561. http://dx.doi.org/10.2110/jsr.2015.35.

Price, W., 1974. Simulation of alluvial fan deposition by a random walk model. Water Resour. Res. 10, 263–274.

Pyrcz, M.J., Catuneanu, O., Deutsch, C.V., 2005. Stochastic surface-based modeling of turbidite lobes. AAPG Bullet. 89, 177–191.

Renard, P., Allard, D., 2013. Connectivity metric for subsurface flow and transport. Adv. Water Res. 51, 168–196. http://dx.doi.org/10.1016/j.advwatres.2011.12.001.

Rezaee, H., Mariethoz, G., Koneshloo, M., Asghari, O., 2013. Multiple-point geostatistical simulation using the bunch-pasting direct sampling method. Comp. Geosci. 54, 293–308. http://dx.doi.org/10.1016/j.cageo.2013.01.020.

Rodell, M., Velicogna, I., Famiglietti, J.S., 2009. Satellite-based estimates of groundwater depletion in India. Nature 460, 999–1002. http://dx.doi.org/10.1038/nature08238.

Ronayne, M.J., Gorelick, S.M., 2006. Effective permeability of porous media containing branching channel networks. Phys. Rev. 73, 026305. http://dx.doi.org/10.1103/PhysRevE.73.026305.

Rongier, G., Collon-Drouaillet, P., Filipponi, M., 2014. Simulation of 3D karst conduits with an object-distance based method integrating geological knowledge. Geomorphology 217, 152–164. http://dx.doi.org/10.1016/j.geomorph.2014.04.024.

Sheets, B.A., Hickson, T.A., Paola, C., 2002. Assembling the stratigraphic record: depositional patterns and time-scales in an experimental alluvial basin. Basin Res. 14, 287–301. http://dx.doi.org/10.1046/j.1365-2117.2002.00185.x.

Singh, A., Paul, D., Sinha, R., Thomsen, K.J., Gupta, S., 2016. Geochemistry of buried river sediments from Ghaggar Plains, NW India: multi-proxy records of variations in provenance, paleoclimate, and paleovegetation patterns in the late quaternary. Palaeogeogr., Palaeoclimatol., Palaeoecol. 449, 85–100. http://dx.doi.org/10.1016/j.palaeo.2016.02.012.

Sinha, R., Ahmad, J., Gaurav, K., Morin, G., 2014. Shallow subsurface stratigraphy and alluvial architecture of the Kosi and Gandak megafans in the Himalayan foreland basin, India. Sed. Geol. 301, 133–149. http://dx.doi.org/10.1016/j.sedgeo.2013.06.008.

Sinha, R., Yadav, G.S., Gupta, S., Singh, A., Lahiri, S.K., 2013. Geo-electric resistivity evidence for subsurface palaeochannel systems adjacent to Harappan sites in northwest India. Quat. Int., 66–75 http://dx.doi.org/10.1016/j.quaint.2012.08.002.

Stauffer, D., Aharony, A., 1992. Introduction to Percolation Theory. second ed.. Taylor & Francis, London.

Stouthamer, E., 2005. Reoccupation of channel belts and its influence on alluvial architecture in the Holocene Rhine-Meuse delta, The Netherlands. In: River Deltas – Concepts, Models, and Examples, Special Publication. SEPM Special Publications, pp. 319–339.

Straub, K.M., Paola, C., Mohrig, D., Wolinsky, M.A., George, T., 2009. Compensational stacking of channelized sedimentary deposits. J. Sed. Res. 79, 673–688. http://dx.doi.org/10.2110/jsr.2009.070.

Strebelle, S., 2002. Conditional simulation of complex geological structures using multiple-point statistics. Math. Geol. 31, 1–21. http://dx.doi.org/10.1023/A:1014009426274.

Sylvester, Z., Pirmez, C., Cantelli, A., 2011. A model of submarine channel-levee evolution based on channel trajectories: implications for stratigraphic architecture. Mar. Petrol. Geol. 28, 716–727. http://dx.doi.org/10.1016/j.marpetgeo.2010.05.012.

Van Dijk, W.M., Densmore, A.L., Singh, A., Gupta, S., Sinha, R., Mason, P.J., Joshi, S.K., Nayak, N., Kumar, M., Shekhar, S., Kumar, D., Rai, S.P., 2016. Linking the morphology of fluvial fan systems to aquifer stratigraphy in the Sutlej-Yamuna plain of northwest India. J. Geophys. Res. – Earth Surf. 121, 201–222. http://dx.doi.org/10.1002/2015JF003720.

Van de Lageweg, W.I., Schuurman, F., Shimizu, Y., Cohen, K.M., Van Dijk, W.M., Kleinhans, M.G., 2016a. Preservation of meandering river channels in uniformly aggrading channel belts. Sedimentology 63, 586–608. http://dx.doi.org/10.1111/sed.12229.

Van de Lageweg, W.I., Van Dijk, W.M., Box, D., Kleinhans, M.G., 2016b. Archimetrics: a quantitative tool to predict three-dimensional meander belt sand-body heterogeneity. Deposit. Rec. 2, 22–46. http://dx.doi.org/10.1002/dep2.12.

Weissmann, G.S., Carle, S.F., Fogg, G.E., 1999. Three-dimensional hydrofacies modeling based on soil surveys and transition probability geostatistics. Water Resour. Res. 35, 1761–1770.

Weissmann, G.S., Hartley, A.J., Scuderi, L.A., Nichols, G.J., Davidson, S.K., Owen, A., Atchley, S.C., Bhattacharjee, P., Chakraborty, T., Ghosh, P., Nordt, L.C., Michel, L., Tabor, N.J., 2013. Prograding distributive fluvial systems – geomorphic models and ancient examples. In: Driese, S.G., Nordt, L.C., McCarthy, P.J. (Eds.), New Frontiers in Paleopedology and Terrestrial Paleoclimatology, pp. 131–147. http://dx.doi.org/10.2110/sepmsp.104.1.

Willis, B.J., Tang, H., 2010. Three-dimensional connectivity of point-bar deposits. J. Sed. Res. 80, 440–454. http://dx.doi.org/10.2110/jsr.2010.046.

Wingate, D., Kane, J., Wolinsky, M., Sylvester, Z., 2015. A new approach for conditioning process-based geological models to well data. Math. Geosci., 1–27 http://dx.doi.org/10.1007/s11004-015-9596-8.

Wu, J., Boucher, A., Zhang, T., 2008. A SGeMS code for pattern simulation of continuous and categorical variable: FILTERSIM. Comput. Geosci. 34, 1863–1876. http://dx.doi.org/10.1016/j.cageo.2007.08.008.